1   Stellar Structure

Enrique García–Berro[1,2] · *Leandro G. Althaus*[3,4]
[1]Departament de Física Aplicada, Universitat Politècnica de Catalunya, Castelldefels, Spain
[2]Institut d'Estudis Espacials de Catalunya, Barcelona, Spain
[3]Facultad de Ciencias Astronómicas y Geofísicas, Universidad Nacional de La Plata, La Plata, Argentina
[4]CONICET-UNLP, La Plata, Argentina

Abstract: In this chapter the equations of stellar structure are introduced. Up-to-date descriptions of the most relevant microphysics needed to build reliable stellar configurations are also provided. These include the equation of state, nuclear reactions, opacities, and other less frequently discussed physical processes, such as diffusion and radiative levitation. The necessary numerical techniques currently employed to build evolutionary stellar models as well as the otherwise necessary boundary conditions needed to integrate the equations of stellar structure are also addressed. Finally, an overview of the current state-of-the-art modeling is given.

1 Introduction

Stars are the fundamental blocks upon which galaxies, and by extension the universe, are built. As such, their study has received continuous interest during several decades. In fact, reliable and up-to-date stellar evolutionary models are routinely required in several fields of modern astrophysics. Hence, understanding the structure of stars is a must, and most branches of astrophysics rely on detailed stellar models. In particular, understanding the structure and evolution of our galaxy, a prototypical spiral galaxy, requires obtaining significant information from statistical studies of the several galactic populations (disk, halo, and bulge). Future space missions, of which Gaia is the archetypical example (Perryman et al. 2001), will obtain an accurate census of the stars in our galaxy, will determine three-dimensional velocities for most of them, and will also quantitatively map its structure. This wealth of information can be accurately and efficiently analyzed only if realistic stellar evolutionary models, based on an accurate description of the properties of stars, are employed. Thus, understanding in detail the structure of stars is of crucial importance. Additionally, Galactic satellite galaxies are proving to be the most natural and successful places where to test and quantify the nature and distribution of dark matter, a key issue in modern cosmology. A precise understanding of these galaxies is a challenge for which again accurate stellar models are needed. Also, the origin of the different chemical elements cannot be assessed without fully understanding the structure and evolution of stars. As a matter of fact, it turns out that all the elements – but hydrogen, helium, lithium, beryllium, and boron – have been synthetized in the deep interiors of stars. Thus, our understanding of the chemical evolution of the universe relies on our ability to describe the details of the internal structure of stars. Moreover, due to the extreme pressures and temperatures that are reached in some of their evolutionary stages, stars can also be used as astroparticle physics laboratories – see the review of Raffelt (1999) – and provide environments that cannot be attained in terrestrial laboratories. Also, stars can be used to test alternative theories of gravitation – see the recent review of García-Berro et al. (2007) – a very hot topic. Finally, a detailed description of stellar structure is also of primordial importance to understand one the most energetic events in our universe: supernovae. Although important, these are only a few examples for which a detailed knowledge of stellar structure is required and there are several other important applications that are omitted here for the sake of conciseness.

As mentioned, our understanding of stellar structure has been built over several decades. To the best of our knowledge the pioneering studies were done, among others, by Lane (1869), Schwarzschild (1906), and Eddington (1916) between the end of the nineteenth century and the very beginning of the twentieth century. Of course, these initial studies were very crude

and several approximations done in these studies have turned out to be inaccurate. Nevertheless, they helped in setting the stage and they contributed to the foundation of a new branch of astronomy. Since then, the field has experimented notable advances and has reached a degree of maturity and a predictive power that do not have other fields of astronomy. Big steps forward were given by renowned astronomers, of which Chandrasekhar, Fowler, Bethe, Schatzman, Sugimoto, Iben, and several others are conspicuous examples. Their work settled the basements of the modern theory of stellar structure. More recently, the advent of computers and of advanced numerical techniques helped to develop a consistent, coherent, and very detailed theory corpus that nowadays has made possible to compare theoretical models with the extremely large amount of very precise data that is routinely acquired by modern large telescopes.

The study of stellar structure involves several fields of contemporary physics. In order to understand the structure of stars several physical inputs are required. Among them nuclear reactions, which are of fundamental importance to understand the energetics of stars, need to be mentioned first. In turn, an accurate knowledge of nuclear reactions involves not only a proper theoretical description of the structure of nuclei, but also large experimental efforts to measure the cross sections of the most important nuclear reactions. Needless to say that although there exist accurate determinations for several nuclear reactions there are still several others for which reliable determinations are sorely needed. Examples of the former are the nuclear reaction rates relevant for hydrogen burning, and the most paradigmatic example of the latter is, perhaps, the $^{12}\text{C}(\alpha, \gamma)^{16}\text{O}$ nuclear cross section. A detailed knowledge of the equation of state of astrophysical plasmas is also required to accurately model stellar structures. This includes not only the description of the thermodynamical properties of the ideal plasma for a wide range of densities and temperatures – see ❯ *Fig. 1-1* – but also, if realistic models are to be computed, several nonideal effects must also be taken into account. Also partial ionization must be carefully taken into account. Accurate modeling of energy losses via neutrino emission requires also a good description of weak interactions. Matter at very large densities, like those found in the interiors of neutron stars, require modeling strong interactions. On the other hand, opacities and conductivities of matter are also required. Actually, the list of physical inputs is so large that no attempt is made to be exhaustive at this point, and a detailed discussion of all the most important physical inputs is deferred to subsequent sections.

Before going into the details of stellar structure modeling it is rather convenient to have an approximate and simplistic, but rather effective, idea of how typical stars, of which our own Sun is an example, work. In fact, a main sequence star can be defined as a self-contained, self-controlled, auto-gravitating thermonuclear reactor – something that nuclear engineers have not been able to reproduce on Earth yet. Assume that all stars have spherical symmetry. This is not an unrealistic assumption, because gravity only depends on distance, but it has been only proved for the case of the closest star: our Sun. The most important property (besides isotropy) of gravity is that it is always attractive, contrary to what happens with electromagnetic interactions. In fact, and as it will be shown in subsequent chapters, the life of a star is a battle against gravity. Actually, normal stars succeed in winning successive battles but they lose the war, exploding as supernovae, the most massive ones, or ejecting their external layers and forming compact objects (either white dwarfs or neutron stars), the less massive ones. Since stars seem to be in equilibrium, a force must balance gravity. This force, obviously, is pressure or, to be more precise, the pressure gradient. That is, Archimede's principle comes at work. Given the densities and temperatures of main sequence stars – see ❯ *Fig. 1-1* – the pressure can be well described by that of a totally ionized ideal gas. This is the same to say that the pressure is proportional to the density (ϱ) and the temperature (T). Now, to balance the gravitational force there are
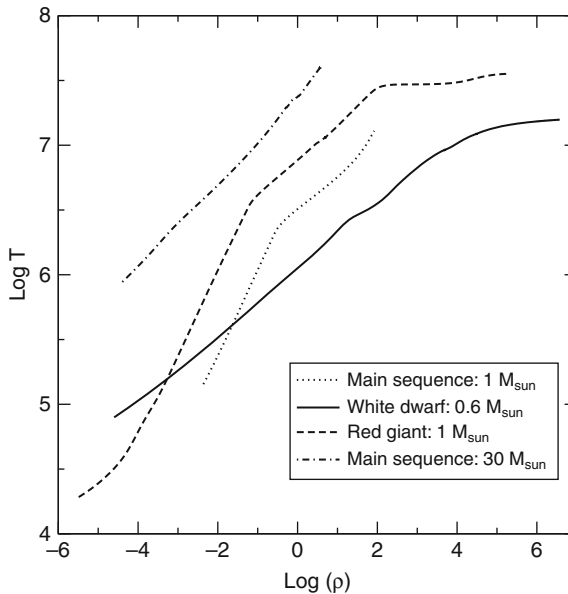
◨ Fig. 1-1
**Structure of several stellar configurations in the density-temperature plane. Note that the loga-
rithms of both quantities are plotted. The most external layers of these stellar configurations are
not displayed. The *dotted line* illustrates the structure of a main sequence star of 1 $M_\odot$. For com-
parative purposes the structure of a main sequence star of 30 $M_\odot$ is also displayed. Both structures
correspond to the moment at which hydrogen is ignited at the center. That is, at the zero age main
sequence. Note that the 30 $M_\odot$ star is considerably hotter than our Sun. Also shown is the structure
of a red giant star of 1 $M_\odot$. As can be seen these types of stars have much wider density and tem-
perature ranges. Actually, the central density of this stellar configuration is rather high. The *solid
line* shows the stratification of densities and temperatures for an otherwise typical white dwarf of
0.6 $M_\odot$. It has been chosen to show the structure at an intermediate evolutionary phase, when the
central temperature is log $T \simeq 7.2$. It is important to realize that the central density in this case is
much larger than in the previous examples**

two possibilities: either to increase the density or to increase the temperature. As increasing
the density increases as well the gravitational force per unit volume, it is rather evident that the
only possibility that is left to play with is the temperature. This has the consequence that since
gravity is stronger at the central regions of the star, the core of a typical main sequence star must
be hotter. The second consequence is that more massive stars must be hotter as well, because
they need to balance an overall stronger gravitational pull. These two facts can be clearly seen
in ❷ *Fig. 1-1*. This issue will be addressed again when the virial theorem, in ❷ Sect. 5, and the
equation of state, in ❷ Sect. 6.1, will be discussed.

Now going one step forward, there is no question that stars shine, that is, stars lose energy.
Thus, as they radiate away energy, stars should cool, the pressure should decrease, and, con-
sequently, the radius should decrease as well. But it turns out that this is not the case. Indeed,
it can be easily shown that the gravitational potential cannot supply the required amount of

energy during long periods of time. Actually, the release of gravitational energy is governed by the Kelvin–Helmholtz timescale:

$$\tau_{KH} \sim \frac{GM^2}{RL} \qquad (1.1)$$

where G is the gravitational constant, $G = 6.674 \times 10^{-8}$ dyn cm^2 g^{-2}, and M, R, and L are, respectively, the total mass, radius, and luminosity of the corresponding star. Adopting the solar values $M = 1\,M_\odot \simeq 1.989 \times 10^{33}$ g, $R = 1\,R_\odot \simeq 6.955 \times 10^{10}$ cm, and $L = 1\,L_\odot \simeq 3.856 \times 10^{33}$ erg s^{-1}, $\tau_{KH} \sim 3.0 \times 10^6$ years is obtained, much shorter than the age of the Solar System, which is ~4.5×10^9 years. Thus, gravitational energy cannot be the source of the luminosity of stars. Therefore, another source of energy must be at work. It took several decades to realize that this source of energy were nuclear reactions occurring in the deep interior of stars. In fact, an indication of this is obtained computing the nuclear timescale:

$$\tau_{nuc} \sim \frac{Mc^2}{L} \qquad (1.2)$$

where c stands for the speed of light, and the rest of the symbols have been already defined. Adopting again typical values, it turns out that $\tau_{nuc} > 10^{10}$ years, which comfortably fits within the age of the Sun. The sketch previously outlined allows to get a preliminary insight of typical stars that will serve as a guide for more quantitative studies. However, it should be emphasized that this sketch is not valid for compact objects, either white dwarfs or neutron stars. For these stars the key control parameter is not temperature, but density, and nuclear reactions become (in most cases and only as far as it is concerned about isolated stars) irrelevant. This issue will be revisited when studying the equation of state.

With all these considerations in mind the study of the subject of this chapter in a consistent manner can be started. The reader should take into account that the purpose of this chapter is not providing a summary of the several stellar evolutionary phases. This will be found elsewhere in this book. Instead, the chapter will focus on detailing all the equations and physical inputs necessary to compute realistic and up-to-date stellar configurations. Also, the reader should be aware that the selection of papers for explicit citation is necessarily somewhat arbitrary, and is the product of the own special research trajectory and interests of the authors.

The chapter is organized as follows. The equations of stellar hydrostatic equilibrium and energy conservation are first introduced. This will be done in ❯ Sects. 2 and ❯ 3, respectively. The main energy transport mechanisms in stars will be described in ❯ Sect. 4. With these tools at hand, an overview of the gross properties of a star, the virial theorem, will be given in ❯ Sect. 5. All the necessary physical inputs (equation of state, nuclear reactions, opacities, and neutrino emission rates) will be provided in ❯ Sect. 6. A brief introduction to other physical processes relevant for stellar evolutionary calculations, like diffusion and radiative levitation, will be given in ❯ Sect. 7. A discussion of how the boundary conditions are usually dealt with will be provided in ❯ Sect. 8, and numerical techniques to compute stellar evolution will be detailed in ❯ Sect. 9. ❯ Section 10 provides insight on modern numerical techniques and available stellar evolutionary codes. Finally, ❯ Sect. 11 will close the chapter providing a brief summary.

2 Hydrostatic Equilibrium

In the absence of rotation and magnetic fields, the only forces acting on a given mass element of an isolated star made of matter plus radiation result from pressure and gravity. For most stars, a spherically symmetric configuration can thus be assumed, where functions are constant on concentric spheres at a distance r from the stellar center. The imbalance between gravitational and differential pressure forces yields the equation of motion at r:

$$\varrho \ddot{r} = -\frac{dP}{dr} - \frac{Gm\varrho}{r^2}, \tag{1.3}$$

where $\ddot{r}$ is the local acceleration d^2r/dt^2, ϱ and P are the local matter density and pressure, and m is the mass in the sphere interior to r. Generally speaking, and for most phases of stellar evolution, stars evolve so slowly that the temporal evolution of the stellar structure can be described by a sequence of models in hydrostatic equilibrium. This being the case, the structure can be assumed to be static. Hence, all time derivatives can be neglected. In this case, the internal pressure gradient balances gravity everywhere in the star, and the equation of motion, (❯ 1.3), reduces to the equation of hydrostatic equilibrium:

$$\frac{dP}{dr} = -\frac{Gm\varrho}{r^2} \tag{1.4}$$

and mass conservation reads:

$$\frac{dm}{dr} = 4\pi r^2 \varrho. \tag{1.5}$$

These two expressions allow to derive an estimate of the central pressure, P_c, of our Sun using dimensional analysis:

$$\frac{P_c}{R} \sim \frac{GM\langle\varrho\rangle}{R^2} \propto \frac{GM^2}{R^5} \tag{1.6}$$

where $\langle\varrho\rangle$ is the mean density and it has been assumed that the pressure at the surface is much smaller than at the center, a very good approximation. Adopting typical values, $P_c \sim 3.0 \times 10^{15}$ dyn cm^{-2} is obtained.

Clearly, the assumption of hydrostatic equilibrium means that the pressure decreases outward. The departures from hydrostatic equilibrium can be characterized using the dynamical timescale τ_{dyn}, which can be computed neglecting the internal pressure gradient in a gravitationally bound configuration. From (❯ 1.3) it follows that

$$\frac{R}{\tau_{\text{dyn}}^2} \sim \frac{GM}{R^2}, \tag{1.7}$$

thus, we obtain

$$\tau_{\text{dyn}} \sim \frac{1}{\sqrt{G\langle\varrho\rangle}}, \tag{1.8}$$

which is essentially the free-fall timescale. For the Sun τ_{dyn} is about 30 min, for a red giant with $\langle\varrho\rangle = 10^{-6}$ g cm^{-3} about 40 days, and for a white dwarf with $\langle\varrho\rangle = 10^6$ g cm^{-3}, it is on the order of a few seconds. This implies that hydrostatic equilibrium is always very quickly attained.

3 Energy Conservation

Let l be the net energy per second outflowing from a sphere of radius r, that is, the luminosity, and ϵ_{nuc} the nuclear energy released per unit mass per second. In a stationary situation in which nuclear reactions are the only energy source of the star, the exceeding energy per second, dl, leaving a spherical mass shell of radius r, mass dm, and thickness dr is

$$dl = 4\pi r^2 \varrho\, \epsilon_{\mathrm{nuc}}\, dr. \tag{1.9}$$

However, heating (or cooling) of the mass element, and the work of expansion (or compression) of the mass shell also contribute to the energy balance. This means that dl can be nonzero even in the absence of nuclear reactions. Using the first law of thermodynamics, the energy equation can then be written

$$\frac{dl}{dm} = \epsilon_{\mathrm{nuc}} + \epsilon_g, \tag{1.10}$$

where ϵ_g is the gravothermal term per unit mass per second

$$\epsilon_g = -\frac{du}{dt} + \frac{P}{\varrho^2}\frac{d\varrho}{dt}, \tag{1.11}$$

and u is the internal energy per gram. Differentiating the internal energy

$$\frac{du}{dt} = \left(\frac{\partial u}{\partial \varrho}\right)_T \frac{d\varrho}{dt} + \left(\frac{\partial u}{\partial T}\right)_\varrho \frac{dT}{dt}, \tag{1.12}$$

and with the help of the thermodynamic relation

$$\left(\frac{\partial u}{\partial \varrho}\right)_T = \frac{P}{\varrho^2} - \frac{T}{\varrho^2}\left(\frac{\partial P}{\partial T}\right)_\varrho, \tag{1.13}$$

❷ Equation 1.11 can be rewritten as

$$\epsilon_g = \frac{T}{\varrho^2}\left(\frac{\partial P}{\partial T}\right)_\varrho \frac{d\varrho}{dt} - C_V \frac{dT}{dt}, \tag{1.14}$$

where C_V is the specific heat at constant density, $C_V = (\partial u/\partial T)_\varrho$. Making use again of basic thermodynamics, considering that $\varrho = \varrho(P, T)$, and the relation

$$\left(\frac{\partial P}{\partial T}\right)_\varrho = \frac{P\delta}{T\alpha}, \tag{1.15}$$

with α the isothermal compressibility and δ the volume coefficient of expansion, given by

$$\delta = -\left(\frac{\partial \ln \varrho}{\partial \ln T}\right)_P$$

$$\alpha = \left(\frac{\partial \ln \varrho}{\partial \ln P}\right)_T. \tag{1.16}$$

(❷ 1.14) can be cast, after some algebra, in the form

$$\epsilon_g = -C_P \frac{dT}{dt} + \frac{\delta}{\varrho}\frac{dP}{dt}, \tag{1.17}$$

where C_P is the specific heat at constant pressure. In this analysis, the variation of the internal energy resulting from the change of local chemical composition has been neglected.

This contribution is usually small for most stages of evolution, as compared to the release of nuclear energy – see Kippenhahn et al. (1965) – but it is relevant in the case of white dwarf stars where nuclear reactions are effectively extinguished (Isern et al. 1997). The energy equation, (❯ 1.10), then becomes

$$\frac{dl}{dm} = \epsilon_{\text{nuc}} - C_P \frac{dT}{dt} + \frac{\delta}{\varrho} \frac{dP}{dt}. \tag{1.18}$$

Integrating (❯ 1.11) over mass gives the overall gravothermal contributions to the total energy budget. It is apparent that the integration of the first term in ϵ_g yields the time variation of the total internal energy of the star. As it will be shown later, integration over m of the second term yields the time derivative of the total gravitational energy (Ω) of the star (Kippenhahn and Weigert 1990).

4 Energy Transport

4.1 Radiative Transport

One of the mechanisms by which energy is transferred in stellar interiors is radiation, that is, by photons. Generally speaking, radiation is the usual process by which energy is carried away in stars. In stellar interiors, the photon mean free path ℓ_{ph} is very short compared to the typical length scale over which the structure changes. The mean free path of a photon can be easily estimated:

$$\ell_{\text{ph}} = \frac{1}{\kappa_{\text{rad}}\, \varrho}, \tag{1.19}$$

where κ_{rad} is the mean radiative opacity coefficient due to interactions of photons with particles, that is, the radiative cross section per unit mass averaged over frequency. Typical values of κ_{rad} for stellar interiors are $\kappa_{\text{rad}} \approx 1 \text{ cm}^2 \text{ g}^{-1}$. Taking into account the average density of matter in the Sun, $\ell_{\text{ph}} \approx 1$ cm. This is much smaller than the stellar radius, thus implying that matter in stellar interiors is very close to local thermodynamic equilibrium, and that the power spectrum of radiation corresponds to that of a blackbody. The mean free path of photons is also so small that the energy transport by radiation can be treated essentially as a diffusive process, introducing an important simplification in the treatment. In the diffusion approximation, the radiative flux is given by

$$\mathbf{F}_{\text{rad}} = -\frac{4\pi}{3\kappa_{\text{rad}}\, \varrho} \nabla B = -\frac{4\, ac\, T^3}{3\kappa_{\text{rad}}\, \varrho} \nabla T, \tag{1.20}$$

here $B = (ac/4\pi)\, T^4$ is the frequency-integrated Planck function, c the speed of light, and a the radiation density constant ($7.564 \times 10^{-15} \text{ erg cm}^{-3} \text{ K}^{-4}$). In the spherical symmetric case, $\mathbf{F}_{\text{rad}}$ has only a radial component, $|\mathbf{F}_{\text{rad}}| = F_{\text{rad}}$. Thus, $l = 4\pi r^2 F_{\text{rad}}$, and the diffusion equation becomes

$$\frac{dT}{dr} = -\frac{3}{4ac} \frac{\kappa_{\text{rad}}\, \varrho}{T^3} \frac{l}{4\pi r^2}. \tag{1.21}$$

The total energy flux depends on an integral over all radiation frequencies. In the diffusion approximation, the generalization to frequency-dependence leads to the concept of the Rosseland mean opacity, obtained as a harmonic mean of the frequency-dependent opacity. This can

be seen by including in the equation for the radiative flux the frequency dependence

$$F_\nu = -\frac{4\pi}{3\kappa_\nu \varrho} \frac{dB_\nu}{dr} = -\frac{4\pi}{3\varrho} \frac{dT}{dr} \frac{1}{\kappa_\nu} \frac{dB_\nu}{dT}, \tag{1.22}$$

where F_ν is the monochromatic flux of frequency ν, and κ_ν the monochromatic opacity resulting from bound–bound, bound–free, and free–free interactions between radiation and electrons. The total flux is obtained by integrating (❯ 1.22) over frequency

$$F_{\text{rad}} = -\frac{4\pi}{3} \frac{1}{\kappa_{\text{rad}} \varrho} \frac{dT}{dr} \int_0^\infty \frac{dB_\nu}{dT} \, d\nu, \tag{1.23}$$

where κ_{rad} is the Rosseland mean opacity given by

$$\frac{1}{\kappa_{\text{rad}}} = \frac{\int_0^\infty \frac{1}{\kappa_\nu} \frac{dB_\nu}{dT} \, d\nu}{\int_0^\infty \frac{dB_\nu}{dT} \, d\nu}. \tag{1.24}$$

With this definition and observing that

$$\int_0^\infty \frac{dB_\nu}{dT} \, d\nu = \frac{ac}{\pi} T^3, \tag{1.25}$$

(❯ 1.21) is recovered. It is worth noting as well that the radiative flux can be cast in the form

$$F_{\text{rad}} = -D \frac{d(aT^4)}{dr}, \tag{1.26}$$

where aT^4 is the radiation energy density and D is a diffusion coefficient given by

$$D = \frac{c}{3\kappa_{\text{rad}}\varrho} = \frac{1}{3} c \, \ell_{\text{ph}}. \tag{1.27}$$

In stellar atmospheres, the mean free path of photons becomes much larger, and the diffusion approximation is not valid. There, a more complete and detailed treatment of the full radiative transfer problem is required (Mihalas and Mihalas 1984).

4.2 Conductive Transport

Energy can be transferred not only by photons but also by particles via collisions during the random thermal motions of the particles. This becomes particularly relevant at the high densities characteristic of evolved stars, where electron degeneracy increases both the electron velocity and the mean free path substantially, thus making the diffusion coefficient large. Hence, in the case of stellar matter where electrons are degenerate, electron conduction results in a very efficient energy transfer mechanism, superseding in some cases radiative transfer.

The energy flux due to electron thermal conduction can be written in terms of a coefficient of thermal diffusion, D_e, and the temperature gradient as

$$F_{\text{cd}} = -D_e \frac{dT}{dr}. \tag{1.28}$$

It is convenient to define a "conductive opacity" as

$$\kappa_{\text{cd}} = \frac{4\,acT^3}{3D_e\,\varrho}, \tag{1.29}$$

so that the total energy flux carried by both radiation and thermal conduction can be written as

$$F_{\text{tot}} = F_{\text{rad}} + F_{\text{cd}} = -\frac{4\,ac\,T^3}{3\kappa_{\text{tot}}\,\varrho}\,\frac{dT}{dr}, \tag{1.30}$$

where the total opacity is expressed as

$$\frac{1}{\kappa_{\text{tot}}} = \frac{1}{\kappa_{\text{rad}}} + \frac{1}{\kappa_{\text{cd}}}. \tag{1.31}$$

Note that when $\kappa_{\text{cd}} \gg \kappa_{\text{rad}}$, then $\kappa_{\text{tot}} \simeq \kappa_{\text{rad}}$, and when electron conduction is very efficient, $\kappa_{\text{cd}} \ll \kappa_{\text{rad}}$, $\kappa_{\text{tot}} \simeq \kappa_{\text{cd}}$ is verified.

It is useful to write the diffusion equation, (❱ 1.21), for the radiative plus conductive transport in terms of the radiative temperature gradient for a star in hydrostatic equilibrium, ∇_{rad},

$$\nabla_{\text{rad}} = \left(\frac{d\ln T}{d\ln P}\right)_{\text{rad}}, \tag{1.32}$$

in the form

$$\nabla_{\text{rad}} = \frac{3}{16\pi acG}\,\frac{\kappa_{\text{tot}}\,l\,P}{m\,T^4}. \tag{1.33}$$

It should be noted that ∇_{rad}, which is a spatial derivative that relates the variables P and T in two close mass shells, describes the temperature variation with depth for a star in hydrostatic equilibrium where energy is transferred by radiation (and conduction).

4.3 Convective Transport

In a stellar interior, energy is transferred not only by radiation and/or conduction, but also by convection, which is also responsible for chemical element transport. Under certain circumstances, small, local perturbations of elements around their equilibrium positions may grow, thus leading to macroscopic motions. These large-scale motions, or convection, lead to energy transport from the hottest to the coolest regions due to the rising and falling of mass elements under the combined action of buoyancy and gravity. The condition for stability of a mass element that is displaced around its equilibrium position in a certain region of a star (due to, for instance, temperature fluctuations) is

$$\left(\frac{d\varrho}{dr}\right)_{\text{int}} > \left(\frac{d\varrho}{dr}\right)_{\text{ext}}, \tag{1.34}$$

where the subscript "int" denotes the change of internal density of the mass element while it rises a distance dr, and the subscript "ext" indicates the spatial gradient in the star. This condition assumes that the element remains always in pressure equilibrium with the surroundings. That is, the element moves with a speed lower than the local sound speed. The stability condition given by (❱ 1.34) simply states that after moving a distance dr, the element will be denser than the fluid in its new environment, so the gravitational force will make the element sink back to its original position.

1

Stellar Structure

In order to translate this stability condition into a more tractable form, the equation of state $\varrho = \varrho(P, T, \mu)$ can be used, and can be written as

$$
\frac{d\varrho}{\varrho} = \frac{P}{\varrho}\left(\frac{\partial\varrho}{\partial P}\right)\frac{dP}{P} + \frac{T}{\varrho}\left(\frac{\partial\varrho}{\partial T}\right)\frac{dT}{T} + \frac{\mu}{\varrho}\left(\frac{\partial\varrho}{\partial\mu}\right)\frac{d\mu}{\mu}
$$

$$
= \alpha\frac{dP}{P} - \delta\frac{dT}{T} + \varphi\frac{d\mu}{\mu}, \tag{1.35}
$$

where α and δ are given by ($\circleddash$ 1.16), μ is the mean molecular weight, and φ is the chemical potential. Hence, the stability criterion becomes

$$
\left(\frac{\alpha}{P}\frac{dP}{dr} - \frac{\delta}{T}\frac{dT}{dr} + \frac{\varphi}{\mu}\frac{d\mu}{dr}\right)_{\text{int}} > \left(\frac{\alpha}{P}\frac{dP}{dr} - \frac{\delta}{T}\frac{dT}{dr} + \frac{\varphi}{\mu}\frac{d\mu}{dr}\right)_{\text{ext}}. \tag{1.36}
$$

Since the element is in equilibrium with its surroundings (the pressure is the same), and the values of α and δ for the fluid element are almost equal to the external ones, the first term on either side of the inequality cancel each other. Also, $(du/dr)_{\text{int}} = 0$ since the element does not change its chemical composition while moving, which is the same to say that there is no matter exchange with the surroundings. Then, ($\circleddash$ 1.36) reduces to

$$
\left(\frac{\delta}{T}\frac{dT}{dr}\right)_{\text{int}} < \left(\frac{\delta}{T}\frac{dT}{dr} - \frac{\varphi}{\mu}\frac{d\mu}{dr}\right)_{\text{ext}}. \tag{1.37}
$$

After multiplying both sides of this inequality by the pressure scale height

$$
\lambda_P = -\frac{dr}{d\ln P}, \tag{1.38}
$$

which is a measure of the distance over which the pressure is changing by a factor e, the stability condition becomes

$$
\left(\frac{d\ln T}{d\ln P}\right)_{\text{ext}} < \left(\frac{d\ln T}{d\ln P}\right)_{\text{int}} + \frac{\varphi}{\delta}\left(\frac{d\ln\mu}{d\ln P}\right)_{\text{ext}}. \tag{1.39}
$$

This condition can be used to test the stability of a layer where all energy is transported by radiation and/or conduction. If the star is stable the term on the left-hand side of ($\circleddash$ 1.39) is the radiative temperature gradient defined by ($\circleddash$ 1.32). It will be assumed that the element moves adiabatically. This is same as assuming that the rising fluid element has no time to exchange its energy content with the surrounding environment. Thus, the Ledoux criterion for dynamical stability is obtained

$$
\nabla_{\text{rad}} < \nabla_{\text{ad}} + \frac{\varphi}{\delta}\left(\frac{d\ln\mu}{d\ln P}\right), \tag{1.40}
$$

where ∇_{ad} is the adiabatic temperature gradient and corresponds to the temperature gradient when the moving element does not exchange heat with the surrounding medium. For a general equation of state, the adiabatic gradient reads

$$
\nabla_{\text{ad}} = \frac{P\delta}{C_P\varrho T}. \tag{1.41}
$$

It is worth mentioning that for the particular case of a chemically homogeneous region of a star, $d \ln \mu / d \ln P = 0$. Therefore, the condition for stability in this case simply reads

$$\nabla_{\mathrm{rad}} \; < \; \nabla_{\mathrm{ad}}, \tag{1.42}$$

which is the Schwarzschild criterion for dynamical stability. In those stellar regions where nuclear reactions produce heavier elements below the lighter ones, the chemical gradient term in (❯ 1.39) favors convective stability since $d \ln \mu / d \ln P > 0$. Indeed, in regions of varying μ, a fluid element moving upward is made of matter with a higher molecular weight than that of its surrounding medium, forcing the element to sink down as a result of gravity.

The derivation of the condition for stability can be seen from a slightly different point of view. Assume that a fluid element in a star is displaced vertically and adiabatically from its equilibrium position with the surroundings at r_0. It will experience a buoyancy force per unit volume equal to $-g \, (\varrho_{\mathrm{int}} - \varrho_{\mathrm{ext}})$, where g is the absolute value of the gravitational acceleration and ϱ_{int} and ϱ_{ext} are, respectively, the interior and exterior densities of the fluid element. In the absence of viscous effects, the equation of motion of the element is

$$\varrho_{\mathrm{int}} \frac{d^2 r}{dt^2} = -g \, (\varrho_{\mathrm{int}} - \varrho_{\mathrm{ext}}). \tag{1.43}$$

For a small displacement $(r - r_0)$, we obtain

$$\varrho_{\mathrm{int}}(r) = \varrho_{\mathrm{int}}(r_0) \; + \; \left(\frac{d\varrho_{\mathrm{int}}}{dr} \right)_{r_0} (r - r_0), \tag{1.44}$$

and the same for ϱ_{ext}. Since at r_0, $\varrho_{\mathrm{int}}(r_0) = \varrho_{\mathrm{ext}}(r_0)$, the equation of motion becomes

$$\varrho_{\mathrm{int}} \frac{d^2 r}{dt^2} + g \left(\frac{d\varrho_{\mathrm{int}}}{dr} - \frac{d\varrho_{\mathrm{ext}}}{dr} \right) (r - r_0) = 0, \tag{1.45}$$

the solution of which is of the form $(r - r_0) = A \exp(i \, N \, t)$, with N the oscillation frequency of the element around its equilibrium position, also called the Brunt–Väisälä frequency, which is given by

$$N^2 = \frac{g}{\varrho} \left(\frac{d\varrho_{\mathrm{int}}}{dr} - \frac{d\varrho_{\mathrm{ext}}}{dr} \right). \tag{1.46}$$

Note that if $(d\varrho_{\mathrm{int}}/dr) > (d\varrho_{\mathrm{ext}}/dr)$, then $N^2 > 0$, N is real, and the movement is oscillatory. These oscillations are also known as gravity waves (not to be confused with gravitational waves in General Relativity) since gravity is the restoring force. Thus, the layer will be stable against convection. On the other hand, if $(d\varrho_{\mathrm{int}}/dr) < (d\varrho_{\mathrm{ext}}/dr)$, then $N^2 < 0$, N is imaginary, and then the element will move exponentially from the equilibrium position. Clearly, the layer will be unstable against convection. Now compare these results with the stability condition given by (❯ 1.34).

The actual temperature gradient in a convective region, the convective gradient ∇_{conv}, will be different from the radiative temperature gradient. It is clear that if a fraction of the total flux is carried by convection, then $\nabla_{\mathrm{conv}} < \nabla_{\mathrm{rad}}$, where ∇_{rad} represents the temperature gradient that would be needed to transport the entire flux by radiation and conduction. The total flux consists of the radiative plus convective fluxes:

$$F_{\mathrm{tot}} = \frac{l}{4\pi r^2} = F_{\mathrm{conv}} + F_{\mathrm{rad}} = \frac{4acGmT^4}{3 \, \kappa_{\mathrm{tot}} \, P \, r^2} \nabla_{\mathrm{rad}}. \tag{1.47}$$

If $\nabla_{\rm conv}$ is the actual temperature gradient, it is clear then that the flux carried by radiation is only

$$F_{\rm rad} = \frac{4acGmT^4}{3\,\kappa_{\rm tot}\,P\,r^2}\nabla_{\rm conv}. \tag{1.48}$$

In a convective zone, the following relations are valid (the second inequality is the criterion for convection)

$$\nabla_{\rm rad} > \nabla_{\rm conv} > \nabla_{\rm int} > \nabla_{\rm ad}. \tag{1.49}$$

The calculation of $\nabla_{\rm conv}$ remains a serious issue. In fact, a model for convection must be specified. Convection is essentially a nonlocal and complex phenomenon that involves the solution of the hydrodynamic equations, and it remains a weak point in the theory of stellar evolution. In most stellar applications, a simple local formulation (Böhm-Vitense 1958) called the mixing-length theory (MLT) is used. This crude model assumes that the convective flux is transported by single size, large fluid elements, which after traveling, on the average, a distance $\ell_{\rm MLT}$, the *mixing length*, break up releasing their energy excess into the surrounding medium. The distance $\ell_{\rm MLT}$, which is also the characteristic size of the elements, is parameterized in terms of the pressure scale height, $\ell_{\rm MLT} = \alpha_{\rm MLT}\,H_P$, where $\alpha_{\rm MLT}$ is a free parameter not predicted by the theory that must be calibrated using observations, and H_P is the pressure scale height. In particular, in the Böhm-Vitense formulation, the MLT involves three length scales which, in most stellar applications, are reduced to $\ell_{\rm MLT}$. Usually, $\alpha_{\rm MLT}$ is found fitting the solar radius ($\alpha_{\rm MLT} \approx 1.6$), and this value is usually used to model other stars and evolutionary phases.

In the deep interior of stars, convection results from the large values of $\nabla_{\rm rad}$ caused by the strong concentration of nuclear burning near the stellar center, for instance during the core hydrogen burning phase via the CNO cycle in stars somewhat more massive than the Sun. The high densities of these regions make the temperature stratification almost adiabatic, and thus $\nabla_{\rm conv} = \nabla_{\rm ad}$. This means that a very small excess of $\nabla_{\rm conv}$ over the adiabatic value is enough to transport all the flux. Consequently, the uncertainties in the MLT theory become irrelevant and a detailed treatment of convection is not required to specify $\nabla_{\rm conv}$. For the Sun, typical convective velocities are of the order of $400\,{\rm cm\,s^{-1}}$, whereas for more massive stars they are much larger. Hence, the turnover time, or the travel time of the elements over the distance $\ell_{\rm MLT}$, ranges from about 1 to 100 days. This time is far much shorter than the main sequence lifetime. In fact, during most evolutionary phases convective mixing is essentially an instantaneous process, thus leading to chemically homogeneous convective zones. However, this may not be true during fast evolutionary stages, where the convective timescale becomes comparable to the evolutionary timescale.

A complete solution of the MLT, with all its associated uncertainties, is required in the low-density, outermost part of convective envelopes where the temperature gradient markedly differs from the adiabatic value (Cox and Giuli 1968). In these layers, large values of $\nabla_{\rm rad}$ result from the large opacity values in the ionization zones of hydrogen and helium close to the surface, causing convection in the outer parts of relatively cool stars. Here, the density and the heat content of matter are so low that a temperature gradient largely exceeding $\nabla_{\rm ad}$ is required to transport energy. Depending on the efficiency of convection, $\nabla_{\rm conv}$ will be somewhere between $\nabla_{\rm ad}$ and $\nabla_{\rm rad}$. Typical values for the average convective velocity in the solar envelope are about $1\,{\rm km\,s^{-1}}$, close the local sound speed, and the turnover timescale is of the order of 5 min.

However, processes such as overshooting, that is, the extension of convective zones beyond the formally convective boundaries given by (❯ 1.40) – at the convective boundaries, fluid

elements have zero acceleration but nonzero velocity – cannot be satisfactorily treated using a local theory. More mixing than is expected from the MLT treatment is supported by different pieces of astrophysical evidence, which suggest that real stars have larger convective cores. Overshooting – which is critical in determining the total amount of nuclear fuel available for the star – is a nonlocal process, and its extent depends on the properties of the adjacent layers. In most studies of stellar structure and evolution, overshooting is simulated extending the boundaries of the convective layer and mixing material beyond the formal convective boundary. This is known as instantaneous overshooting. A better approach is to treat overshooting as a diffusion process. This approach enables a self-consistent treatment of this process in the presence of nuclear burning (Herwig 2000). Here, overshooting parameterization is based on hydrodynamical simulations (Freytag et al. 1996), which show that turbulent velocities decay exponentially outside the convective boundaries. This diffusive overshooting gives rise to mixing in the overshoot regions whose efficiency is quantified in terms of the diffusion coefficient

$$D_{\text{os}} = D_0 \, \exp\left(\frac{-2\,z}{H_{\text{v}}}\right), \tag{1.50}$$

where D_0 is the diffusion coefficient at the boundary of the convection zone, z is the radial distance from the edge of the convection zone, and H_{v} is the velocity scale height of the overshoot convective elements at the convective boundary. H_{v} is parameterized as a fraction f of the pressure scale height, $H_{\text{v}} = f\,H_P$. The parameter f is a measure of the extent of the overshooted region. Clearly, the larger the f, the extra mixing beyond the convective boundary extends further. Usually $f \approx 0.016$ is adopted. This choice of f accounts for the observed width of the main sequence as well as for the intershell abundances of hydrogen-deficient post-AGB remnants.

Another complication is the occurrence of "semiconvection," a slow mixing process that is expected to occur in those regions with an inward increasing value of μ that are unstable according to the Schwarzschild criterion but stable according to the Ledoux criterion, namely, those layers where

$$\nabla_{\text{ad}} + \frac{\varphi}{\delta}\left(\frac{d\ln\mu}{d\ln P}\right) > \nabla_{\text{rad}} > \nabla_{\text{ad}}. \tag{1.51}$$

Here, energy losses from the fluid elements (elements are hotter than the surroundings) will cause them to oscillate around their equilibrium positions (vibrational instability) with progressively growing amplitudes (Kippenhahn and Weigert 1990). Because of heat losses, the elements return to the equilibrium position with a temperature lower than that with which they started, thus reaching deeper and hotter regions in their downward excursion. The growth of the oscillation amplitudes is determined by the timescale of thermal adjustment of the fluid elements. The overstability resulting from these growing oscillations and nonlinear effects is believed to result in partial mixing of the corresponding layers. Realistic physical models of all these nonlocal processes require two- and three-dimensional numerical simulations of nonlinear hydrodynamic instabilities and turbulent processes (Young et al. 2003). Finally, heat leakage of the elements is also responsible for another type of instability, thermohaline convection. This process leads to significant turbulent transport in stable regions with negative chemical gradients – see Traxler et al. (2011) for recent three-dimensional simulations of this process in stars.

In closing, it is worth mentioning that various attempts to improve the MLT have been made. In particular, Canuto and Mazzitelli (1991) have considered the full spectrum of turbulence in velocities and sizes of the convective eddies. An extended version of the Mixing Length Theory of convection, for fluids with composition gradients, has been derived by Grossman and

Taam (1996) in the local approximation. These authors – see also Grossman et al. (1993) – have developed the nonlinear Mixing Length Theory of double diffusive convection (GNA), where both the effects of thermal and composition gradients compete to determine the stability of the fluid. The GNA theory is based on the MLT picture and considers the fluid as an ensemble of individual elements or blobs. This ensemble is described by a distribution function that evolves in time according to a Boltzmann-type equation. In its local version, all third-order terms in the second-moment of the Boltzmann equation are neglected. The GNA theory applies in convective, semiconvective, and thermohaline regimes. According to this treatment, the diffusion coefficient D characterizing mixing in the various regimes is given by

$$D = \frac{1}{3}\ell\sigma \tag{1.52}$$

where $\ell = \alpha H_P$ is the mixing length and σ the turbulent velocity. The value of σ is determined by simultaneously solving the equations for the turbulent velocity and flux conservation – see Grossman and Taam (1996) for further details. In this theory of convection, the standard MLT for a fluid of homogeneous composition is a limiting case.

5 The Virial Theorem

Stars are one of the best examples of a virialized system. In fact, it is rather simple to prove this. Assume that they are in hydrostatic equilibrium – and, hence, that (❱ 1.4) holds – and that they are made up of an ideal gas. Accordingly, multiplying (❱ 1.4) by $4\pi r^3$ and integrating over the entire star,

$$\int_0^R 4\pi r^3 \frac{dP}{dr}dr = -\int_0^R 4\pi r^3 \frac{G\varrho m}{r^2}dr \tag{1.53}$$

is obtained, where R is the stellar radius. The left-hand side of this equation can be easily worked out. Integrating by parts it is found that

$$\int_0^R 4\pi r^3 \frac{dP}{dr}dr = \left[4\pi r^3 P\right]_0^R - 3\int_0^R P4\pi r^2 dr = -3\int_0^M \frac{P}{\varrho}dm \tag{1.54}$$

where it has been assumed that the pressure at the surface of the star vanishes, and (❱ 1.5) has been used. The right-hand side of the previous equation can also be further worked out, to yield

$$-\int_0^R 4\pi r^3 \frac{G\varrho m}{r^2}dr = -\int_0^R 4\pi r^2 \varrho\frac{Gm}{r}dr = -\int_0^R \frac{Gm}{r}dm = \Omega \tag{1.55}$$

which is the total gravitational energy. Thus,

$$3\int_0^M \frac{P}{\varrho}dm + \Omega = 0. \tag{1.56}$$

Quite generally, for an ideal gas, $P = (\gamma - 1)\varrho u$, where u is the internal energy and γ is the adiabatic index. Thus, substituting this relationship in the last equation, a rather general result is obtained:

$$3(\gamma - 1)U + \Omega = 0 \tag{1.57}$$

where the total thermal energy, U, has been introduced. On the other hand, the total energy of a star (the binding energy) is $B = U + \Omega$. Thus,

$$B = \frac{3\gamma - 4}{3\gamma - 3}\Omega. \tag{1.58}$$

For a perfect gas $\gamma = 5/3$. Consequently, $2U + \Omega = 0$ and $B = \Omega/2$. This means that if a star contracts – or, equivalently, it releases gravitational energy – half of the gravitational energy is transformed in thermal energy, whereas the other half must be radiated away. Note as well that since $\Omega < 0$, the total energy of the star is also negative, an otherwise expected result that means that the star is bound. Only in the case in which $\gamma = 4/3$, that is, for a completely degenerate relativistic gas, $B = 0$. This last result is of special significance as it is closely related to the concept of Chandrasekhar's mass and to the explosion mechanism of thermonuclear supernovae.

The virial theorem can be used to obtain a relation between the stellar mass and the mean temperature, T. Assume that stars are essentially composed of hydrogen. This assumption is valid for most stars, for which the hydrogen mass fraction is typically ~0.75. The total thermal energy is thus

$$U \sim \frac{3}{2} N k_{\mathrm{B}} T \propto MT \tag{1.59}$$

where N is the total number of particles and $k_{\mathrm{B}} = 1.380\,\mathrm{erg\,K^{-1}}$ is the Boltzmann constant. Since $\Omega \propto -GM^2/R$ and $U = -\Omega$, it follows that $T \propto M/R$, and thus the more massive a star, the hotter, in qualitative agreement with arguments put forth in ❯ Sect. 1. This argument can be pushed forward to obtain a mass-luminosity relationship. The total luminosity of a star can be expressed as $L = 4\pi R^2 F$, where F is the flux. Using (❯ 1.20) we obtain:

$$F \propto \frac{1}{\kappa \varrho} T^3 \frac{dT}{dr} \sim \frac{1}{\kappa \varrho} \frac{T^4}{R}. \tag{1.60}$$

Consequently, after some elementary algebra, and taking into account that the virial theorem states that $T \propto M/R$, and also considering that $\varrho \propto M/R^3$ one arrives at the conclusion that $L \propto M^3/\kappa$. This is same as saying that more massive stars are not only hotter, but also more luminous.

6 Physical Inputs

As has been shown in the previous sections, the basic equations describing the structure and evolution of stars are relatively simple. To this description the microphysics, that is, the properties of stellar matter, has to be added. These properties include the equation of state, opacity, and energy generation rates, among others. The relevant processes occur in an interacting plasma of ions, electrons, and atoms, and the detailed physics of these processes is still an active field of research. Thus, some uncertainties still remain. In this section, all the main physical inputs necessary to model the structure of a star are detailed. These include, of course, the equation of state, described in ❯ Sect. 6.1, which provides the pressure as a function of the temperature, density, and chemical composition. Obviously this is needed to solve the equation of hydrostatic equilibrium. The second important input is the nuclear energy generation rate – ❯ Sect. 6.2 – which, as mentioned, is needed to maintain stable temperatures during long periods of time. Attention will be paid to only the most important thermonuclear reaction rates, namely, to those relevant for the hydrogen, helium, and carbon burning phases, and other interesting nuclear reactions will be briefly mentioned, but the aim of this section is not to be exhaustive. The interested reader is referred to the several recent works on this particular topic – see, for instance, the detailed and interesting paper of Longland et al. (2010) and subsequent publications – for detailed and exhaustive information. As already shown, opacities and conductivities are crucial in evaluating the rate at which energy is transported, and they are described

in ❯ Sect. 6.3, while ❯ Sect. 6.4 is devoted to describe the most recent neutrino emission rates. Finally, in ❯ Sect. 7 an overview will be given of the several other physical inputs which are only required under special circumstances.

6.1 Equation of State

The equation of state describes the thermodynamical properties of stellar matter and relates density to pressure, temperature, and chemical composition. It is particularly simple in the case of an ideal gas, but physical processes relevant for stars – that include, among others, ionization, electron degeneracy, molecular dissociation, radiation pressure, or Coulomb interactions – turn the treatment of the equation of state into a rather complex issue. In dealing with these effects, care must be taken to ensure the treatment to be thermodynamically consistent in the sense that it satisfies the thermodynamical identities between the different quantities. One way in which this can be achieved consists in deriving the equation of state from the free energy of the gas. Using this approach, the thermodynamical state of the gas for a given temperature, density, and composition is derived minimizing the free energy, which yields the occupation numbers and ionization states. The relevant thermodynamical quantities can be then obtained as derivatives of the free energy. This is the basis for the so-called chemical picture in determining the equation of state. The second way to ensure thermodynamical consistency is based on the physical picture. Within this less used approach, instead of dealing with the chemical equilibrium of a set of predefined ions, atoms, and molecules, only elementary particles of the problem (nuclei and electrons) are assumed at the beginning, and composite particles appear as a result of the interactions in the system.

It is customary to characterize the chemical composition of stellar matter by means of the mean molecular weight, μ, defined as $\mu = \varrho/(n\,m_H)$, where n is the total number of particles per unit volume and m_H the atomic mass unit (1.6605×10^{-24} g). For a mixture of fully ionized gases, the molecular weight of the gas is given by the harmonic mean of the molecular weights of the ions (μ_o) and electrons (μ_e):

$$\frac{1}{\mu} = \frac{1}{\mu_o} + \frac{1}{\mu_e}, \tag{1.61}$$

where

$$\frac{1}{\mu_o} = \sum_i \frac{X_i}{A_i}, \tag{1.62}$$

$$\frac{1}{\mu_e} = \sum_i \frac{X_i\,Z_i}{A_i}, \tag{1.63}$$

with X_i, A_i, and Z_i being the mass fraction (normalized to unity), $X_i = \varrho_i/\varrho$, atomic weight, and charge, respectively, of element i. These definitions are apparent by noting that

$$n = \frac{\varrho}{\mu m_H} = n_e + n_o = \sum_i Z_i n_i + \sum n_i = \sum_i Z_i \frac{X_i}{A_i m_H}\varrho + \sum_i \frac{X_i}{A_i m_H}\varrho, \tag{1.64}$$

where n_i is the number of ions per unit volume of element i. In the case of a neutral gas, the molecular weight reduces to μ_o. For complete ionization, a simple expression for μ_e is obtained

by assuming that for all elements heavier than helium ($Z > 2$), $A_i/Z_i \approx 2$. In this case the molecular weight per electron becomes

$$\mu_e = \frac{2}{1 + X_\mathrm{H}},$$ (1.65)

where X_H is the abundance by mass of hydrogen. In this approximation and when there is no hydrogen, $\mu_e = 2$.

6.1.1 Ions

In the absence of quantum effects, and assuming that the potential energy of particle interactions is much smaller than the kinetic energy of the particles, the equation of state of ions adopts the simplest form. The particles obey the Maxwell–Boltzmann distribution, and the equation of state corresponding to an ideal (perfect) gas results

$$P = \frac{k_\mathrm{B}}{m_\mathrm{H}\mu} \varrho\, T.$$ (1.66)

This equation describes the equation of state of fully ionized matter, as found in the deep interior of stars (note that the electron contribution is through μ), as well as matter where all electrons are in the atom (no ionization at all).

If photons contribute appreciably to gas pressure, $P_\mathrm{rad} = (1/3)\,a\,T^4$, then the equation of state becomes (assuming that radiation is in thermodynamic equilibrium with matter)

$$P = \frac{k_\mathrm{B}}{m_\mathrm{H}\,\mu} \varrho\, T \;+\; \frac{1}{3} a T^4.$$ (1.67)

From the internal energy per unit mass of the monoatomic gas (it is assumed that, in the case of neutral matter, there are no internal degrees of freedom):

$$E = \frac{3}{2} \frac{k_\mathrm{B}}{m_\mathrm{H}\,\mu}\, T \;+\; \frac{a T^4}{\varrho},$$ (1.68)

the specific heat at constant pressure, C_P, and the adiabatic temperature gradient, ∇_ad, are derived:

$$C_P = \frac{k_\mathrm{B}}{m_\mathrm{H}\,\mu} \left[\frac{3}{2} \;+\; \frac{16 - 12\beta - 3\beta^2}{\beta^2} \right],$$ (1.69)

and

$$\nabla_\mathrm{ad} = \frac{1 + \frac{(1 - \beta)(4 + \beta)}{\beta^2}}{\frac{5}{2} + \frac{4(1-\beta)(4 + \beta)}{\beta^2}}.$$ (1.70)

Here, β quantifies the importance of radiation pressure, and is defined as $\beta \equiv P_{gas}/P$, where P is the total pressure due to gas plus radiation. If radiation pressure is negligible, then $\beta \to 1$ and $P_{gas} \to P$, $C_P \to 5k_B/(2\mu m_H)$, and $\nabla_{ad} \to 0.4$, the well-known values for the ideal gas. For $\beta \to 0$, $P \to P_{rad}$, $C_P \to \infty$, and $\nabla_{ad} \to 0.25$.

This simple treatment ignores a number of important effects that are relevant in the astrophysical context. For instance, at low temperatures, partial ionization of matter must be taken into account. This changes the mean molecular weight and the energetics of the gas. The treatment of partial ionization is usually done assuming chemical equilibrium between the gas constituents. In this case, the ratio n_{j+1}/n_j of atoms $j+1$ times ionized to those which are j times ionized is given by the Saha equation

$$\frac{n_{j+1}}{n_j} = 2\frac{u_{j+1}}{u_j}\left(\frac{2\pi m_e}{h^2}\right)^{3/2}\frac{(k_B T)^{5/2}}{P_e}e^{-\chi_j/k_B T}, \tag{1.71}$$

where u_j is the partition function for the ion in the energy state j (which is a function of T), h is the Planck constant, P_e is the electronic pressure, and χ_j is the ionization energy. Note that ionization is favored at high temperatures and low electronic pressures. Quantities such as C_P, ∇_{ad}, and μ are notably affected by ionization. In particular, ∇_{ad} is decreased below 0.4 and C_P markedly increases when compared with the values resulting from fully ionized perfect gas. It is important to note, however, that the treatment of ionization is a difficult task since it involves considering the various ionization degrees of all chemical species. The problem is specified by a full set of coupled Saha equations, the solution of which can only be done numerically.

6.1.2 Electrons

The inner regions of the vast majority of highly evolved stars, including white dwarf stars, are dominated by degenerate electrons. At very high densities and low temperatures, the de Broglie wavelength of electrons, $h/(2m_e k_B T)^{1/2}$, becomes larger than the mean separation of electrons ($d \sim \varrho^{-1/3}$) and, as a result, quantum effects become relevant. Hence, electrons become degenerate and quantum mechanics – the Pauli exclusion principle – strongly affects the equation of state. In this case, the distribution of electron momenta obeys the Fermi–Dirac statistics, and the average occupation number at equilibrium of a cell in the phase space – actually, the distribution function of energies – is given by

$$f(\varepsilon) = \frac{1}{1 + \exp\left[(\varepsilon - \mu_q)/k_B T\right]}, \tag{1.72}$$

where μ_q is the chemical potential of the gas and ε is the kinetic energy corresponding to the momentum, p, which is given by:

$$\varepsilon(p) = m_e c^2\left[\sqrt{1 + (p/m_e c)^2} - 1\right]. \tag{1.73}$$

Note that this expression is valid for both relativistic and nonrelativistic electrons – in the nonrelativistic limit ($pc \ll m_e c^2$), and $\varepsilon \simeq p^2/2m_e$. For noninteracting, degenerate electrons at

a given temperature T, the number density and pressure for the electron gas are, respectively,

$$n_e = \frac{8\pi}{h^3} \int_0^\infty \frac{p^2}{1 + \exp\left[(\varepsilon - \mu_q)/k_B T\right]}\, dp \tag{1.74}$$

$$P_e = \frac{8\pi}{3h^3} \int_0^\infty \frac{p^3}{1 + \exp\left[(\varepsilon - \mu_q)/k_B T\right]} \frac{d\varepsilon_p}{dp}\, dp. \tag{1.75}$$

In the limit of high temperature and low density, $\mu_q/k_B T \ll -1$, and the distribution function reduces to the Maxwell–Boltzmann distribution, $f(\varepsilon) \to \exp[-(\varepsilon - \mu_q)/k_B T]$. In this case, $P_e \to n_e k_B T$. At very high densities (or very low temperatures), that is, when the de Broglie wavelength is much larger than the mean separation, the electron gas behaves as a zero-temperature gas. In this zero-temperature approximation, $\mu_q \gg k_B T$ and μ_q is identified with the Fermi energy (ε_F). Hence, the Fermi–Dirac distribution that characterizes electrons reduces to the step-like function:

$$f(\varepsilon) = \begin{cases} 1 & \text{if } \varepsilon \le \varepsilon_F \\ 0 & \text{if } \varepsilon > \varepsilon_F. \end{cases}$$

In this situation, electrons occupy only the energy states up to ε_F, and not the higher energy states where the distribution function is zero. In particular, those electrons with energies close to ε_F will make the largest contribution to the pressure. In this zero-temperature approximation, the so-called complete degeneracy approximation, the electron pressure can be easily derived by considering only the energy states up to ε_F. Then, (❷ 1.74) and (❷ 1.75) need only to be integrated up to p_F, the momentum corresponding to the Fermi energy. Using the relation $\varrho = \mu_e m_H n_e$, the electron pressure and mass density become then

$$\begin{aligned} P_e &= \frac{8\pi}{3h^3} \int_0^{p_F} \frac{(p^4/m_e)dp}{\sqrt{1 + (p/m_e c)^2}} \\ &= A\left[x(x^2 + 1)^{1/2}(2x^2 - 3) + 3\sinh^{-1}(x)\right] \\ \varrho &= B\mu_e\, x^3, \end{aligned} \tag{1.76}$$

where the dimensionless Fermi momentum is given by $x = p_F/m_e c$, $A = \pi m_e^4 c^5/3h^3 = 6.0 \times 10^{22}$ dyn cm^{-2}, and $B = 8\pi m_e^3 c^3 m_H/3h^3 = 9.74 \times 10^5$ g cm^{-3}, and the rest of the symbols have their usual meaning. Note that this expression is valid for any relativistic degree (Chandrasekhar 1939). Relativistic effects have to be taken into account at very high densities – note that as the density is increased so does p_F. In particular, relativistic effects start becoming prominent when $p_F \approx m_e c$ or $x \approx 1$, which corresponds to a density of $\varrho/\mu_e \approx 10^6$ g cm^{-3}. This density corresponds to typical values of the central densities in white dwarf stars. Thus, it is expected that electrons in the core of white dwarfs are partially relativistic. Expansions of the equation for the electronic pressure P_e are possible in the limiting cases $x \to 0$, namely, nonrelativistic, and $x \to \infty$, extremely relativistic. In both cases it is possible to eliminate the variable x, thus resulting in simple equations for the pressure of a completely degenerate electron gas:

$$P_e \to A\frac{8}{5}x^5 = \left(\frac{3}{8\pi}\right)^{2/3} \frac{h^2}{5m_e m_H^{5/3}} \left(\frac{\varrho}{\mu_e}\right)^{5/3} \tag{1.77}$$

$$= 1.004 \times 10^{13} \left(\frac{\varrho}{\mu_e}\right)^{5/3} \quad x \ll 1$$

$$P_e \to A \, 2 \, x^4 = \left(\frac{3}{8\pi}\right)^{1/3} \frac{hc}{4m_{\mathrm{H}}^{4/3}} \left(\frac{\varrho}{\mu_e}\right)^{4/3} \tag{1.78}$$

$$= 1.244 \times 10^{15} \left(\frac{\varrho}{\mu_e}\right)^{4/3} \qquad x \gg 1$$

where P_e is in dyn cm^{-2}. Although the zero-temperature approximation is an idealized one, the electron gas in some astrophysical environments behaves as if it were indeed at zero temperature. This is the case of the core of cool white dwarfs, where their structure is supported entirely by the pressure of an almost completely degenerate electron gas. This becomes clear by noting that the condition for complete degeneracy, $T_{\mathrm{F}} \equiv \varepsilon_{\mathrm{F}}/k_{\mathrm{B}} \gg T$, where T_{F} is the Fermi temperature, can be written in the form (for nonrelativistic electrons):

$$T_{\mathrm{F}} = \frac{1}{k_{\mathrm{B}}} \frac{p_{\mathrm{F}}^2}{2m_e} = \frac{m_e c^2}{2k_{\mathrm{B}}} \left(\frac{\varrho}{C}\right)^{2/3} = 3 \times 10^5 \left(\frac{\varrho}{\mu_e}\right)^{2/3} \gg T \,. \tag{1.79}$$

For a typical white dwarf with a central density of $10^7 \, \mathrm{g \, cm^{-3}}$, $T_{\mathrm{F}} = 9 \times 10^9 \, \mathrm{K}$, which is much larger than the core temperature (typical core temperatures range from 10^7 to $10^6 \, \mathrm{K}$). Hence, the electron gas behaves as a zero-temperature Fermi gas. In sharp contrast, at the center of the Sun $\varrho/\mu_e \approx 100$, thus $T_{\mathrm{F}} \approx 6 \times 10^6 \, \mathrm{K}$, smaller than its central temperature ($\sim 10^7 \, \mathrm{K}$). Hence, electron degeneracy is not relevant at the center of the Sun. Finally, note the smaller dependence of pressure on density for relativistic electrons. This relativistic "softening" of the equation of state is responsible for the existence of a limiting mass for white dwarf stars, the so-called Chandrasekhar limiting mass (Chandrasekhar 1939).

As noted, the equation of state of white dwarf interiors can be well approximated by that of an ideal Fermi gas at zero temperature. This has important consequences. In particular, the pressure only depends on the density and not on the temperature. Consequently, the control parameter to balance the gravitational pull in this case is ϱ, at odds with what was discussed in ❯ Sect. 1 for normal stars. It should be reminded that for main sequence stars the control parameter is the temperature, and hence more massive stars have larger temperatures. This is not the case for white dwarfs. Massive white dwarfs have larger central densities. It is easy to also show that more massive white dwarfs have smaller radii and, in the limit, Chandrasekhar's mass appears as the limiting mass for which the radius of the equilibrium configuration is zero.

In the case of finite temperature ($T \neq 0$), the Fermi–Dirac distribution for electrons cannot be approximated by a step-like function as in the case in which complete degeneracy is assumed. Here, $T_{\mathrm{F}} \sim T$ and those electrons with energies near ε_{F} can occupy levels with energies larger than ε_{F}. This situation is referred to as partial degeneracy, and the number density and electron pressure are given by (❯ 1.74) and (❯ 1.75), respectively. Only the case of nonrelativistic electrons, for which $\varepsilon = p^2/(2m_e)$, will be considered here. Introducing the degeneracy parameter $\alpha = -\mu_q/k_{\mathrm{B}}T$, these equations become

$$n_e = \frac{8\pi}{h^3} \int_0^\infty \frac{p^2}{1 + \exp(\alpha + p^2/2m_e k_{\mathrm{B}} T)} \, dp = \frac{4\pi}{h^3} \left(2m_e k_{\mathrm{B}} T\right)^{3/2} F_{1/2}(\alpha), \tag{1.80}$$

$$P_e = \frac{8\pi}{3h^3 m_e} \int_0^\infty \frac{p^4}{1 + \exp(\alpha + p^2/2m_e k_{\mathrm{B}} T)} dp = \frac{8\pi}{3h^3} \left(2m_e k_{\mathrm{B}} T\right)^{3/2} k_{\mathrm{B}} T \, F_{3/2}(\alpha), \tag{1.81}$$

where $F_n(\alpha)$ are the Fermi–Dirac integrals, given by

$$F_n(\alpha) = \int_0^\infty \frac{u^n}{1 + \exp(\alpha + u)}\, du. \tag{1.82}$$

It should be kept in mind that in the case of partial degeneracy, relativistic effects have to be considered for temperatures in excess, 10^9 K. Indeed, it has been shown that relativistic effects for a degenerate gas become relevant when density exceeds $10^6\,\mathrm{g\,cm^{-3}}$. At such densities, degeneracy will be essentially complete unless $T > 10^9$ K. These rather extreme conditions are only found in some very late stages of stellar evolution. Hence, the equation of state in the case of relativistic partial degeneracy will not be discussed, instead the reader is referred to the specialized literature for this specific topic. In particular, it is worth mentioning here that the most commonly used equation of state is the so-called Helmholtz equation of state. Full details of the Helmholtz equation of state are provided in Timmes and Swesty (2000). This implementation of the equation of state includes contributions from radiation, completely ionized nuclei, and degenerate and relativistic electrons; has perfect thermodynamic consistency; and covers the density and temperature ranges $10^{-12} \leq \varrho\,(\mathrm{g\,cm^{-3}}) \leq 10^{15}$ and $10^3 \leq T\,(\mathrm{K}) \leq 10^{13}$, respectively. It is freely available on the Web page of F. X. Timmes,[1] where several additional physical inputs can also be found. Continuing with our treatment, it is immediately clear from (❯ 1.80) to (❯ 1.81) that

$$P_e = n_e k_B T \left[\frac{2}{3} \frac{F_{3/2}(\alpha)}{F_{1/2}(\alpha)} \right]. \tag{1.83}$$

This equation gives the pressure of a nonrelativistic, partially degenerate electron gas. Given ϱ (or n_e) and T, the value of α can be found from (❯ 1.80), and $F_{3/2}(\alpha)$ and P_e can be assessed. Note that the term in brackets in (❯ 1.83) measures the degree to which the pressure of a degenerate electron gas differs from that of a nondegenerate gas. In the nondegenerate limit, $\alpha \to \infty$, the term in brackets tends to 1, and $P_e \to n_e k_B T$. Even for $\alpha > 2$, the electron pressure is basically the pressure of a nondegenerate gas.❯ Equation 1.83 also shows that the transition from the nondegenerate regime to that of complete degeneracy as the density increases is not discontinuous, but instead there is a gradual transition between those extreme conditions.

These and other concepts become clear when an expansion of the Fermi–Dirac integrals is considered. This is possible in the limits of weak and strong degeneracy. For weak degeneracy ($\alpha > 0$) it can be shown that

$$n_e = \frac{2(2\pi m_e k_B T)^{3/2}}{h^3} \sum_{n=1}^\infty (-1)^{n+1} \frac{e^{-n\alpha}}{n^{3/2}} \qquad \alpha > 0, \tag{1.84}$$

$$P_e = \frac{2 k_B T (2\pi m_e k_B T)^{3/2}}{h^3} \sum_{n=1}^\infty (-1)^{n+1} \frac{e^{-n\alpha}}{n^{5/2}} \qquad \alpha > 0. \tag{1.85}$$

Note that for very large values of α, only the first term of each series is relevant, and the classical result $P_e = n_e k_B T$ is recovered. Taking the first two terms of the series, the correction to the pressure of an ideal gas due to very weak degeneracy is

$$P_e = n_e k_B T \left[1 + \frac{n_e h^3}{2^{7/2} (2\pi m_e k_B T)^{3/2}} + \dots \right], \tag{1.86}$$

---

which is valid for large enough α. On the other hand, for strong, but not complete, degeneracy ($\alpha \ll -1$), expansion of the Fermi–Dirac integrals leads to

$$n_e = \frac{8\pi}{3h^3}(2m_e)^{3/2}\mu_q^{3/2}\left[1 + \frac{\pi^2}{8}\left(\frac{k_B T}{\mu_q}\right)^2 + \frac{7\pi^4}{640}\left(\frac{k_B T}{\mu_q}\right)^4 + \ldots\right] \qquad (1.87)$$

$$P_e = \frac{8\pi}{3h^3}(2m_e)^{3/2}\frac{2}{5}\mu_q^{5/2}\left[1 + \frac{5\pi^2}{8}\left(\frac{k_B T}{\mu_q}\right)^2 + \frac{7\pi^4}{384}\left(\frac{k_B T}{\mu_q}\right)^4 + \ldots\right]. \qquad (1.88)$$

These expressions allow to compute some basic thermodynamic quantities. For instance, the specific heat at constant volume

$$C_V = \left(\frac{dE}{dT}\right)_{V,N_e} = \left(\frac{\partial E}{\partial T}\right)_{\mu_q} + \left(\frac{\partial E}{\partial \mu_q}\right)_T \frac{d\mu_q}{dT}, \qquad (1.89)$$

where $E = (3/2)P_e V$ is the internal energy of electrons. Taking into account that $dn_e = 0$ – the volume of the gas is fixed – and considering only the first order in T, it can be shown that the specific heat at constant volume for a almost completely degenerate electron gas is

$$C_V \approx \frac{\pi^2}{2}\frac{k_B T}{\varepsilon_F} \ll 1. \qquad (1.90)$$

Thus, the specific heat for degenerate electrons is proportional to temperature. In the case of strong degeneracy, the specific heat of the electron gas is much smaller than that of an ion gas. This is a somewhat expected result because, as a result of the exclusion principle, only those electrons with energies near the Fermi energy will be able to change its energy as a result of a temperature variation.

Taking into account the contribution of ions and radiation, the equation of state for a mixture of ions, electrons, and radiation can be written

$$P = P_{\rm ion} + P_e + P_{\rm rad} = \frac{k_B}{m_H \mu_o}\varrho\, T + \frac{8\pi}{3h^3}\int_0^\infty \frac{p^3}{1 + \exp\left[(\varepsilon - \mu_q)/k_B T\right]}\frac{d\varepsilon_p}{dp}\, dp + \frac{a}{3}T^4, \quad (1.91)$$

$$\varrho = \mu_e m_H \frac{8\pi}{h^3}\int_0^\infty \frac{p^2}{1 + \exp\left[(\varepsilon - \mu_q)/k_B T\right]}\, dp. \qquad (1.92)$$

Note that ions are treated as a Maxwell–Boltzmann gas. This is so because at any given temperature ions require much higher densities than electrons to become degenerate – because of their larger mass, the de Broglie wavelength corresponding to ions is much shorter than that of electrons. For strong degeneracy, ions barely contribute to the total pressure. As a matter of fact, the stronger the degeneracy, the smaller the contribution of the ion gas to the total pressure. However, ions mostly contribute to the mass density (note the presence of m_H in the equation for density) and strongly influence the thermodynamic properties of the mixture as well.

6.1.3 Nonideal Effects

The ion and electron equations of state just described have to be modified in the presence of interactions between particles. In particular, at high densities and low temperatures, Coulomb

interactions modify the thermodynamic properties of the ion gas, and in particular the specific heat. The strength of Coulomb interactions – relative to the thermal kinetic energy – is determined by the Coulomb coupling parameter, which is defined as:

$$\Gamma = \frac{(Ze)^2}{a k_B T} = 0.2275 \frac{Z^2}{T_8} \left(\frac{\varrho_6}{A} \right)^{1/3} \tag{1.93}$$

where T_8 is the temperature in units of 10^8 K, ϱ_6 is the density in units of 10^6 g cm^{-3}, and a is the radius of the Wigner–Seitz sphere:

$$a = \left(\frac{4\pi}{3} n_i \right)^{-1/3}, \tag{1.94}$$

n_i being the number density of ions. For small values of Γ, Coulomb forces are of minor importance (relative to thermal motions) and the ions behave like an ideal noninteracting gas. But, once Γ becomes of order unity, ions begin to undergo short-range correlations, eventually behaving like a liquid. For large enough values of Γ (~180), as usually found in the core of cool white dwarfs, they form a lattice structure. Coulomb interactions between the charged particles of the gas make a negative contribution to the pressure and at low densities affect the energetics and ionization states. Various types of interactions between the constituents have to be taken into account in a realistic treatment that eventually leads to "pressure ionization." Neglecting these interactions and considering only a simple treatment of ionization given by the Saha equation – see (❯ 1.71) – leads to the incorrect prediction that matter at the center of the Sun is far from being completely ionized. Sophisticated equations of state for solar-type stellar interior conditions are those of Mihalas et al. (1988) and OPAL (Rogers and Iglesias 1992; Rogers et al. 1996), based on the chemical and physical picture, respectively, whereas for cool white dwarfs the most up-to-date treatment can be found in Segretain et al. (1994) and references therein.

6.2 Nuclear Reactions

6.2.1 General Concepts

Consider a generic reaction between a particle a and a nucleus X to produce a nucleus, Y and a particle b. Usually, both a and b can be either another nucleus, a photon, a proton, a neutron, or an α particle. These are the most common reactions in stellar interiors, although not the only ones since at very large densities electron captures may also play a role. A symbolic way of expressing this is

$$a + X \rightarrow Y + b \tag{1.95}$$

although in a short and more convenient notation this is frequently expressed as $X(a, b)Y$. In all nuclear reactions charge, nucleon number, momentum, and energy must be conserved. However, the sum of the masses of the reactants differs from the sum of the masses of the products. The difference is called the mass excess. The mass excess is linked to the binding energy E_B of the nuclei involved in the nuclear reaction. Consider a nucleus of mass number A, charge Z, and mass $M(A, Z)$. The binding energy – that is, the energy required to separate the nucleons against their mutual attraction by the strong nuclear forces – is defined as

$$E_B = \left[(A - Z) m_n + Z m_p - M(A, Z) \right] c^2, \tag{1.96}$$

and the binding energy per nucleon is E_B/A. The mass excess is then

$$\Delta M = M_a + M_X - M_b - M_Y = \Delta E_B/c^2, \tag{1.97}$$

where ΔE_B is the difference of binding energy of the reaction products and reactants. This energy difference is released in exothermic nuclear reactions and is responsible for keeping stable the temperature in stellar interiors. For instance, when hydrogen is burned to form helium, four hydrogen nuclei are converted in one helium nucleus. Given the masses of the proton and of a helium nucleus, 26.5 MeV are released in the process, corresponding to just 0.7% of the rest mass of the system. The binding energy increases as a function of mass number, peaks for ^{56}Fe, and then decreases. Thus, exothermic reactions are either the consequence of thermonuclear fusion of light nuclei or of fission of nuclei heavier than ^{56}Fe into lighter ones. The former constitutes the main energy source in stars, provided that the temperatures are sufficiently high to overcome the Coulomb barrier of the interacting particles. On the other hand, endothermic nuclear reactions are only produced in those environments where an excess of thermal energy is available.

6.2.2 Thermonuclear Reaction Rates

The nuclear reaction rate between two nuclei can be expressed as:

$$r_{aX} = \frac{n_a n_X}{1 + \delta_{aX}} \langle \sigma v \rangle_{aX} = \frac{1}{1 + \delta_{aX}} \frac{\varrho^2 N_A^2 X_a X_X}{A_a A_X} \langle \sigma v \rangle_{aX}, \tag{1.98}$$

where the Kronecker δ prevents from counting twice identical particles, n_a and n_X are the number densities of the reacting particles, X_a and X_X are the corresponding mass fractions, N_A is Avogadro's number, and $\langle \sigma v \rangle_{aX}$ is the product of the nuclear cross section, σ, and the relative velocity, v, of the intervening nuclei, averaged over the distribution of relative velocities. At the densities and temperatures typical of stellar interiors the distribution of velocities of the interacting nuclei can be well approximated by a Maxwellian thermal distribution, because at the relevant conditions found in most stars ions are nondegenerate:

$$\langle \sigma v \rangle_{aX} = \sqrt{\frac{8}{\pi \mu (k_B T)^3}} \int_0^\infty E \sigma(E) \exp\left(-\frac{E}{k_B T}\right) dE \tag{1.99}$$

where E is the relative kinetic energy, and μ is the reduced mass of the colliding nuclei. For nonresonant reactions induced by charged particles the astrophysical S-factor, $S(E)$, is usually introduced instead of the nuclear cross section:

$$\sigma(E) = \frac{S(E)}{E} \exp\left[-2\pi\eta(E)\right], \tag{1.100}$$

where $\eta(E) = Z_a Z_X \alpha/v$ is the Sommerfeld parameter, and α is the fine structure constant. The exponential factor measures the probability of penetration of the Coulomb barrier. This is done because the $S(E)$ is a smoothly varying function and can be better extrapolated to low energies, the regions where most of the relevant nuclear reactions occur. Accordingly, after a

Taylor expansion, one finally obtains

$$\langle \sigma v \rangle_{aX} = \sqrt{\frac{2}{\mu k_B T}} \frac{\Delta E_0}{k_B T} f_0 S_{\text{eff}} \exp\left(-\frac{3E_0}{k_B T}\right)$$

$$= 1.301 \times 10^{-14} \text{ cm}^3 \text{ s}^{-1} \left(\frac{Z_a Z_X}{A}\right)^{1/3} f_0 \frac{S_{\text{eff}}}{\text{MeV b}} T_9^{-2/3} \exp\left(-\frac{3E_0}{k_B T}\right), \quad (1.101)$$

where the energy of the Gamow peak E_0 – that is, the energy where the integrand of (❯ 1.99) adopts its maximum value, and thus the reaction is most probable – is given by

$$\frac{E_0}{k_b T} = \left(\frac{\pi Z_a Z_X \alpha}{\sqrt{2}}\right)^{2/3} \left(\frac{\mu}{k_B T}\right)^{1/3}, \quad (1.102)$$

and the full width at half maximum of the integrand is

$$\frac{\Delta E_0}{k_B T} = 4\sqrt{\frac{E_0}{3k_B T}} \quad (1.103)$$

and

$$A = \frac{A_a A_X}{A_a + A_X}. \quad (1.104)$$

Finally,

$$S_{\text{eff}} = S(0)\left(1 + \frac{5k_B T}{36E_0}\right) + S'(0)E_0\left(1 + \frac{35k_B T}{36E_0}\right) + \frac{1}{2}S''(0)E_0^2\left(1 + \frac{89k_B T}{36E_0}\right) + \dots \quad (1.105)$$

and T_9 is the temperature in units of 10^9 K. The factor f_0 accounts for the electron screening and will be discussed later. Hence, the values that need to be measured experimentally (or, in the cases where this is impossible, theoretically computed) are $S(0)$, $S'(0)$, and $S''(0)$.

This formulation is only valid for nonresonant reactions. However, there are several nuclear reactions in which there is a resonance. This happens when the energy of the interacting nuclei is coincident with the energy level of an intermediate nucleus that eventually decays to produce the daughter nuclei:

$$a + X \rightarrow Z \rightarrow Y + b. \quad (1.106)$$

When this occurs, the nuclear reaction rate is enhanced by several orders of magnitude. For the sake of simplicity, and without any loss of generality, it will be assumed that particle Z has only one single excited state and that, moreover, can only decay to particles a and X and b and Y. The probability of these transitions is given by the corresponding lifetimes, τ_a and τ_b, which can be easily expressed by the inverse of the partial widths of the resonance in the incident and exit channels, Γ_a and Γ_b. Thus, the probability of the direct reaction is Γ_b/Γ, where $\Gamma = \Gamma_a + \Gamma_b$, while that of the backward reaction is Γ_a/Γ. In this case it can be shown that the cross section of the resonant nuclear reaction is given by the well-known Breit–Wigner formula:

$$\sigma_{aX}(E) = \pi \lambda^2 \omega \frac{\Gamma_a \Gamma_b}{(E - E_0)^2 + (\Gamma/2)^2}, \quad (1.107)$$

where $\lambda = \hbar/p$, $p = \sqrt{2\mu E}$ is the momentum, E is the energy of the colliding particles, E_0 is the mean energy of the resonance, and

$$\omega = \frac{2J + 1}{(2J_a + 1)(2J_X + 1)} \quad (1.108)$$

is a statistical factor that takes into account the angular momenta of the intervening particles, J is the total angular momentum of the resonant state, and J_a and J_X are the corresponding angular momenta of particles a and X. Obviously, (❯ 1.107) shows that the closer the energy to the mean energy of the resonance, the more likely the reaction. Thus, averaging over the Maxwellian distribution, we obtain

$$\langle \sigma_{aX} \rangle = \sqrt{\frac{8}{\mu\pi}} \left(\frac{1}{k_B T} \right)^{3/2} \int_0^\infty E \sigma_{aX}(E) \exp\left(-\frac{E}{k_B T} \right) dE, \tag{1.109}$$

which, taking into account that the resonances are usually very narrow, and thus the Maxwellian distribution barely changes over the width of the resonance, can be very well approximated by:

$$\langle \sigma_{aX} \rangle = \sqrt{2\pi} \left(\frac{1}{\mu k_B T} \right)^{3/2} \omega \hbar^2 \Gamma_a \Gamma_b \exp\left(-\frac{E_0}{k_B T} \right) \int_0^\infty \frac{dE}{(E - E_0)^2 + (\Gamma/2)^2}, \tag{1.110}$$

which, after some elementary algebra, reduces to:

$$\langle \sigma_{aX} \rangle = \hbar^2 \left(\frac{2\pi}{\mu k_B T} \right)^{3/2} \left(\omega \frac{\Gamma_a \Gamma_X}{\Gamma} \right) \exp\left(-\frac{E_0}{k_B T} \right), \tag{1.111}$$

which, in combination with (❯ 1.98), provides the thermonuclear rate.

6.2.3 Electron Screening

The thermonuclear reaction rates previously explained assume that the reacting particles are isolated. In fact, in stellar interiors this is not true, as the plasma is totally ionized. Thus, around each nuclei there is a cloud of electrons that shields the positive charges, hence lowering the Coulomb barrier and enhancing the reaction rates. Consequently, the nuclear reaction rates derived in ❯ Sect. 6.2.2 must be conveniently modified to account for this. This is done using a multiplicative factor, f. Here, it will be outlined how this screening factor is computed.

In the weak-screening approximation (valid in the case of low densities) the modified electrostatic potential is given by (Salpeter 1954):

$$V(r) = \frac{\alpha Z_a Z_X}{r} e^{-r/r_{\rm DH}}, \tag{1.112}$$

where all the symbols but the Debye–Hückel radius have been already defined:

$$r_{\rm DH} = \sqrt{\frac{k_B T}{4\pi \zeta e^2 \varrho N_A}}, \tag{1.113}$$

being

$$\zeta = \sum_i \frac{Z_i(Z_i + 1)}{A_i} x_i, \tag{1.114}$$

where x_i is the number abundance of chemical species i, with charge Z_i and atomic mass number A_i.

The weak-screening approximation holds when the average interaction energy between particles is smaller than the mean particle kinetic energy. In this case the thermonuclear

reaction rate is enhanced by a factor:

$$\ln f = \frac{Z_a Z_X e^2}{r_{\mathrm{DH}} k_{\mathrm{B}} T} \simeq 0.188 Z_a Z_X \sqrt{\frac{\zeta \varrho}{T_6^3}}, \tag{1.115}$$

where T_6 is the temperature in units of 10^6 K.

In the case of strong screening (large densities), however, this expression is no longer valid, and another approximation must be used. For the sake of conciseness the formulation of Itoh et al. (1990) will be closely followed, and for simplicity a one-component plasma will also be assumed. For extremely dense stellar plasmas the enhancement factor is computed from two important parameters that characterize dense plasmas: the Coulomb coupling parameter Γ, given by (❯ 1.93), and

$$\tau = \left[\left(\frac{27\pi^2}{4} \right) \frac{A m_p (Ze)^4}{\hbar^2 k_{\mathrm{B}} T} \right]^{1/3}, \tag{1.116}$$

where m_p is the proton mass. This parameter gives the classical turning point at the Gamow peak $r \simeq 3\Gamma/\tau$. In this analysis the electrons are assumed to be strongly degenerate. That is, it is assumed that $T \ll T_{\mathrm{F}}$, where T_{F} is the Fermi temperature, and furthermore the ions are treated as classical particles. Accordingly, their thermal de Broglie wavelength

$$\Lambda = \frac{2\pi\hbar^2}{A m_p k_{\mathrm{B}} T} \tag{1.117}$$

verifies the condition $n_i \Lambda^3 \leq 1$. Under these conditions the enhancement factor is given by:

$$\ln f = 1.25\Gamma - \tau h(\beta), \tag{1.118}$$

where

$$h(\beta) = \frac{0.0455\beta + 0.348\beta^3 + 9.49\beta^6 - 0.123\beta^{12} + 0.101\beta^{13}}{1 + 100\beta^4 + 0.267\beta^{12}}, \tag{1.119}$$

with $\beta = 3\Gamma/\tau$.

6.2.4 Nuclear Networks

Nuclear reactions not only release energy but also change the chemical composition of the stellar interior. This is an important issue as chemical composition changes are an important driver of stellar evolution. Accordingly, the necessary equations to follow the change of chemical composition must be added to the set equations presented in ❯ Sects. 2–4. The change of molar abundances $Y_i = n_i/\varrho N_{\mathrm{A}}$ with time due to nuclear processes is followed using a set of coupled ordinary differential equations. If N is the number of chemical species, the nuclear network has a size N^2. A typical reaction network reads:

$$\frac{dY_i}{dt} = \frac{1}{\varrho N_{\mathrm{A}}} \left(- \sum_j Y_j Y_i \lambda_j + \sum_{kl} Y_k Y_l \lambda_{kl} - \frac{Y_i}{\tau_i} + \dots \right). \tag{1.120}$$

The first term in (❯ 1.120) corresponds to the net destruction of nucleus i due to its interaction with nucleus j, while the second one corresponds to the creation of nucleus i from nuclear reactions involving nuclei k and l. The third term in this equation is the spontaneous radioactive

decay of nuclei i with timescale τ_i. As can be seen the nuclear reaction equations constitute a set of first-order, nonlinear differential equations. In most stellar evolutionary codes, (❯ 1.120) is discretized in a convenient way and the chemical changes are obtained inverting a matrix. For the sake of conciseness, it is assumed that nuclear decays can be neglected. If the beginning and the end of the time interval are denoted by superscripts n and $n+1$, then (❯ 1.120) can be linearized and expressed as (Arnett and Truran 1969)

$$Y_i^{n+1}\left(\frac{1}{\Delta t} + Y_j^n \lambda_{ij}\right) + Y_j^{n+1} Y_i^n \lambda_{ij}^n - Y_k^{n+1} Y_l^n \lambda_{kl}^n - Y_l^{n+1} Y_k^n \lambda_{kl}^n = Y_k^n Y_l^n \lambda_{kl}^n - Y_i^n Y_j^n \lambda_{ij}^n \quad (1.121)$$

where Δt is the adopted time step. This set of equation can be solved by the Gauss method. Nevertheless, adequate time steps must be chosen. Typically,

$$\Delta t \le \eta \frac{Y_i^n}{(dY_i/dt)^n} \quad (1.122)$$

where η is a constant less than unity. Typical values for this constant range from 0.01 to 0.05.

6.2.5 Hydrogen Burning Reactions

The energy source of main sequence stars is hydrogen burning, and the reaction product is helium. The total energy yield of this nuclear reaction is 26.73 MeV. Depending on whether a star occupies the lower or the upper main sequence, hydrogen burning occurs through the pp-chains or the CNO cycle. For the reader unfamiliar with this terminology, it should be noted that massive stars are located in the upper main sequence, whereas low-mass stars populate the lower main sequence. There are three pp-chains, and in all of them the first step involves a weak interaction to form deuterium and an $e^- e^+$ annihilation:
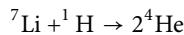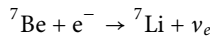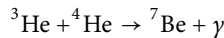
$$^1H + {}^1H \rightarrow {}^2H + e^+ + \nu_e$$
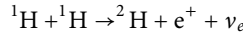
In a second step an isotope of helium is formed:

$$^2H + {}^1H \rightarrow {}^3He + \gamma.$$
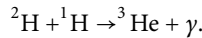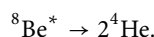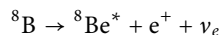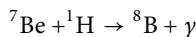
Once enough ^3He is accumulated it follows the so-called pp-I chain:

$$^3He + {}^3He \rightarrow {}^4He + 2{}^1H.$$
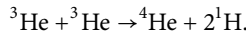
However, for the temperatures typical of main sequence stars ^3He is also burned through the pp-II chain:

$$^3He + {}^4He \rightarrow {}^7Be + \gamma$$
$$^7Be + e^- \rightarrow {}^7Li + \nu_e$$
$$^7Li + {}^1H \rightarrow 2{}^4He$$

or the pp-III chain, in which an excited state of beryllium decays to form two helium nuclei:

$$^3He + {}^4He \rightarrow {}^7Be + \gamma$$
$$^7Be + {}^1H \rightarrow {}^8B + \gamma$$
$$^8B \rightarrow {}^8Be^* + e^+ + \nu_e$$
$$^8Be^* \rightarrow 2{}^4He.$$
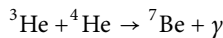
The pp-II chain starts to be relevant for temperatures above $\sim 1.4 \times 10^7$ K, while the pp-III chain operates for temperatures larger than $\sim 2.3 \times 10^7$ K. Finally, it is important to realize that all the nuclei involved in these chains but helium and hydrogen are very unstable, so the interactions are rather inefficient. Actually, the CNO cycle is a more efficient way to produce helium. In fact, CNO cycle is a bi-cycle: the CN cycle, which is dominant for relatively low temperatures, and the NO cycle, which operates mostly for larger temperatures. Both cycles need a seed of carbon, nitrogen, and oxygen to be operative, and these nuclei catalyze the conversion of hydrogen into helium. To begin with, the CN cycle is described next:

$$^1\text{H} + {}^{12}\text{C} \rightarrow {}^{13}\text{N} + \gamma$$
$$^{13}\text{N} \rightarrow {}^{13}\text{C} + e^+ + \nu_e$$
$$^1\text{H} + {}^{13}\text{C} \rightarrow {}^{14}\text{N} + \gamma$$
$$^1\text{H} + {}^{14}\text{N} \rightarrow {}^{15}\text{O} + \gamma$$
$$^{15}\text{O} \rightarrow {}^{15}\text{N} + e^+ + \nu_e$$
$$^1\text{H} + {}^{15}\text{N} \rightarrow {}^{12}\text{C} + {}^{12}\text{He} + \gamma.$$
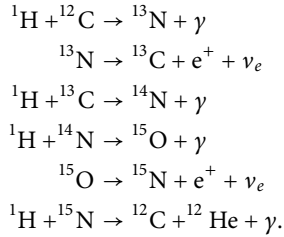
In this cycle the reaction with the smallest cross section, which acts as a bottleneck, is the fourth one. Thus, in equilibrium the overall rate is governed by the reaction rate of ^{14}N. Also, the last reaction of the CN cycle can be substituted by this suite of nuclear reactions:

$$^1\text{H} + {}^{15}\text{N} \rightarrow {}^{16}\text{O} + \gamma$$
$$^1\text{H} + {}^{16}\text{O} \rightarrow {}^{17}\text{F} + \gamma$$
$$^{17}\text{F} \rightarrow {}^{17}\text{O} + e^+ + \nu_e$$
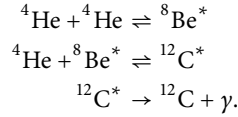$$^1\text{H} + {}^{17}\text{O} \rightarrow {}^{14}\text{N} + {}^4\text{He} + \gamma$$
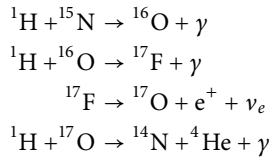
which is known as the ON cycle. According to the previous discussion, the equilibrium CNO abundances are determined by the nuclear cross section of ^{14}N, and thus the CNO cycle also converts carbon and oxygen into nitrogen. Perhaps, the most commonly used reaction rates for all this suite of reactions are those of Caughlan and Fowler (1988), although there are more recent prescriptions – see, for instance, Adelberger et al. (2011).
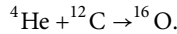
6.2.6 Helium Burning Reactions

Once hydrogen is exhausted in the core of a main sequence star, the pressure gradient cannot be balanced by the energy release of nuclear reactions. Hence, the hydrogen-exhausted core contracts, and becomes hotter. At the same time a hydrogen burning shell is established, the envelope expands, and the star becomes a red giant. Moreover, the envelope becomes convectively unstable and the products of nuclear reactions produced deep in the star are dredged-up to the surface. This is perhaps the most convincing proof of our ability to correctly understand the fine details of stellar structure and evolution, because the theoretically computed abundances of most of the nuclear species match those observationally found. When the temperature reaches $T \sim 10^8$ K helium is ignited through the so-called triple-alpha process, and contraction stops. This nuclear reaction can actually be regarded as a three-body interaction, thereby its name,

and not a normal nuclear reaction. The suite of reactions is

$$^4\mathrm{He} + {}^4\mathrm{He} \rightleftharpoons {}^8\mathrm{Be}^*$$
$$^4\mathrm{He} + {}^8\mathrm{Be}^* \rightleftharpoons {}^{12}\mathrm{C}^*$$
$$^{12}\mathrm{C}^* \rightarrow {}^{12}\mathrm{C} + \gamma.$$

Note that the nuclear isotope $^8\mathrm{Be}^*$ is very short-lived at these very high temperatures. This is the reason why this reaction is usually considered a three-body interaction, and also why as soon as some carbon is produced α captures on it rapidly set in:

$$^4\mathrm{He} + {}^{12}\mathrm{C} \rightarrow {}^{16}\mathrm{O}.$$

Thus, the reaction products of helium burning are carbon and oxygen, the ratio between their abundances being extremely dependent on the temperature at which burning proceeds. As mentioned previously, the $^{12}\mathrm{C}(\alpha, \gamma)^{16}\mathrm{O}$ reaction rate is the subject of a vivid debate, as it is one of the most poorly determined experimentally. The nuclear cross section relies on an extrapolation to low energies of the experimental data, which involves several resonances. Since this cross section is crucial in several stellar evolutionary stages, this constitutes a serious drawback of the theory. The most commonly employed nuclear reaction rates of this set of nuclear reactions are those of the NACRE compilation (Angulo et al. 1999).

6.2.7   Carbon Burning Reactions

Once helium is exhausted in the inner regions of the star, its core can no longer support its own gravitational force, and consequently starts to contract again until the temperatures necessary to burn carbon are reached. This occurs at $T \sim 7 \times 10^8$ K. At the same time the star climbs the so-called asymptotic giant branch in the Hertzsprung–Russell diagram. Carbon burning only occurs for stars with masses larger than ~8 $M_\odot$ (García-Berro et al. 1997; Ritossa et al. 1996). The nuclear reaction network involved in the carbon burning phase is shown in ❱ *Fig. 1-2*. As can be seen, the number of nuclear isotopes largely increases, and several isotopes of carbon, nitrogen, oxygen, neon, sodium, and magnesium are involved. The most relevant reactions are, nevertheless, the carbon–carbon reaction, yielding either neon or magnesium, and α and proton and neutron captures. The most recent and up-to-date nuclear reaction rates for these last reactions are those of Rauscher and Thielemann (2000, 2001) and Iliadis et al. (2010), whereas in most stellar evolutionary codes the prescription of Caughlan and Fowler (1988) is usually adopted for the fusion of two carbon nuclei.

6.2.8   Other Nuclear Reactions of Interest

After carbon exhaustion there are several other nuclear burning stages. These burning stages only occur for stars with mass larger than ~11 $M_\odot$ – see, for instance, Ritossa et al. (1999). These burning stages include neon photo-disintegration, oxygen burning, and silicon burning. Neon is burned before oxygen because at the very high temperatures required to overcome the Coulomb barrier of oxygen atoms (~2.0 × 10^9 K), $^{20}\mathrm{Ne}$ is photo-disintegrated:

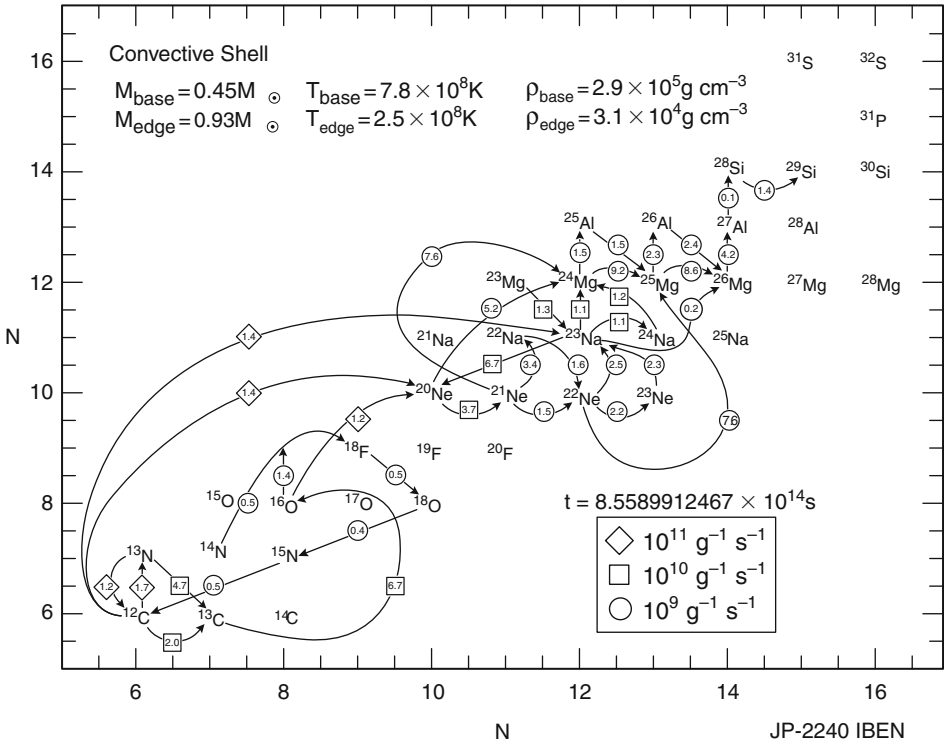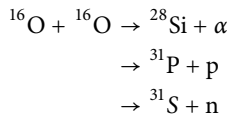$$^{20}\mathrm{Ne} + \gamma \rightleftharpoons {}^{16}\mathrm{O} + \alpha. \tag{1.123}$$

◘ Fig. 1-2
Nuclear reaction network for carbon burning. From García-Berro et al. (1997)

This reaction occurs at $T \sim 1.9 \times 10^9$ K and is usually followed by an α capture (using the α particles liberated in the photo-disintegration) on ^{20}Ne to produce ^{24}Mg:

$$^{20}\text{Ne} + \alpha \rightarrow {}^{24}\text{Mg} + \gamma. \tag{1.124}$$

Consequently, the products of neon photo-disintegration are oxygen and magnesium, plus some other products (sodium, zinc, aluminum, silicon, etc.) with much smaller abundances. After neon is exhausted the next nuclear burning stage is oxygen burning:

$$
\begin{aligned}
^{16}\text{O} + {}^{16}\text{O} &\rightarrow {}^{28}\text{Si} + \alpha \\
&\rightarrow {}^{31}\text{P} + p \\
&\rightarrow {}^{31}\text{S} + n
\end{aligned}
$$

plus the corresponding recaptures of p, n, and α particles. The final products are mainly ^{28}Si and ^{32}S, and traces of ^{33,34}S, ^{35,37}Cl, ^{36,38}Ar, ^{39,41}K, and ^{40,42}Ca.

Finally, the last major burning stage is silicon burning. This burning stage involves a very complex network of fast photo-disintegrations, with all sorts of reaction products (protons, neutrons, and α particles), and the corresponding back-reactions. The main products of silicon burning are iron-peak nuclei. However, it is worth mentioning that, at odds with all the previous burning stages, silicon burning occurs at such high temperatures ($T \sim 3.5 \times 10^9$ K) that reactions

are in quasi-equilibrium. This means that the reactions between the intervening nuclei are so fast that the abundances of such nuclei are close to Nuclear Statistical Equilibrium. Under these conditions the typical reactions are photo-disintegrations to produce neutrons, protons, and α particles, plus the corresponding (γ, α), (n,α), (p,α), and (n,p) reactions – that is, a chain of reactions which are all in equilibrium. Using basic thermodynamical relations the equilibrium abundances can be obtained:

$$n(Z,A) = \frac{g(Z,A)A^{3/2}}{2^A} n_p^Z n_n^{A-Z} \left(\frac{2\pi\hbar^2}{m_p k_B T} \right)^{-\frac{3}{2(A-1)}} \exp\left(\frac{E_B(Z,A)}{k_B T} \right) \tag{1.125}$$

where g is the nuclear partition function and the rest of the symbols have been previously defined. To solve this equation the conditions of baryon and charge conservation must also be added. It turns out that in nuclear statistical equilibrium – see, for instance Bravo and García-Senz (1999), and references therein – the composition of matter is essentially determined by the density, the temperature, and the electron fraction, $Y_e = n_e/n$, which is basically the proton-to-nucleon ratio.

6.3 Opacities and Conductivities

6.3.1 Radiative Opacities

As previously discussed in ❯ Sect. 4, in stellar interiors the diffusion approximation is valid and the temperature gradient is proportional to the Rosseland mean opacity, obtained as a harmonic mean of the frequency-dependent opacity – see (❯ 1.31). Accordingly, opacity is a crucial physical property of stellar matter, since it determines the rate at which energy is transferred from the interior to the outer space. Opacity calculations rely on very detailed descriptions of the interaction between the radiation field and the stellar matter. In fact, bound–free, bound–bound, and free–free interactions between photons and electrons are significant sources of opacity. In turn, these processes depend on the detailed thermodynamical state of the gas, in particular, on the detailed distribution of electrons on the energy levels of the atoms. Consequently, the equation of state plays a major role in the calculation of the opacity.

At high temperatures, when stellar material is almost completely ionized, the main source of opacity is electron scattering with photons. Under these conditions, the cross section for the interaction of photons with electrons is that of Thomson scattering:

$$\sigma_e = \frac{8\pi}{3} \left(\frac{e^2}{m_e c^2} \right)^2 = 0.66 \times 10^{-24} \, \text{cm}^2. \tag{1.126}$$

From this equation, the opacity due to electron scattering is computed as $\kappa_e = \sigma_e n_e / \varrho$. Given that $n_e = \varrho/(\mu_e m_H) = 0.5\varrho(1 + X_H)/m_H$, it follows that

$$\kappa_e = 0.2 \, (1 + X_H) \, \text{cm}^2 \, \text{g}^{-1}. \tag{1.127}$$

Note that in the case of complete ionization, this opacity source is independent of the temperature and density. Since κ_e is independent of frequency, (❯ 1.127) provides the Rosseland mean for electron scattering. However, at high enough temperatures, when photons are sufficiently energetic ($k_B T \sim m_e c^2$), the exchange of momentum between electrons and photons has to be considered, thus reducing somewhat the opacity.

The second important source of opacity are free–free transitions. In this case absorption of radiation occurs when a free electron approaches an ion of charge Z. The physical principle operating in this case is quite simple: As an electron passes close to an ionized atom it can be accelerated or decelerated, respectively, absorbing or emitting a photon in the process. Since the photon can be of any wavelength, radiation emitted in this way has a continuous spectrum. These processes can be studied from a classical point of view. It can be shown that the absorption coefficient is proportional to $Z^2 v^{-3}$ per ion. At a temperature T, the electron thermal velocity is $v^2 \sim T$. Consequently the time interval during which the electron is close enough to the ion scales as $v^{-1} \sim T^{-1/2}$. Moreover, at a density ϱ, the number of electron–ion pairs able to take part in the process scales as ϱ, and therefore the contribution to the opacity scales as $\sim \varrho T^{-1/2}$. Since the absorption coefficient per system is proportional to $Z^2 v^{-3}$, it follows that

$$\kappa_{\mathrm{ff}}^{v} \sim Z^2 \varrho\, T^{-1/2} v^{-3}. \tag{1.128}$$

Thus, the resulting approximate Rosseland opacity due to this process only turns out to be

$$\kappa_{\mathrm{ff}} = 3.68 \times 10^{22} (X_{\mathrm{H}} + X_{\mathrm{He}})(1 + X_{\mathrm{H}})\, \varrho\ T^{-7/2}\, \mathrm{cm}^2\, \mathrm{g}^{-1}, \tag{1.129}$$

which is often referred to as the Kramers opacity. In this expression X_{He} is the abundance by mass of helium.

Absorptions of photons by bound electrons with the result that electrons are removed from the atoms or ions (the so-called bound–free transitions) constitutes another important source of continuum opacity. In the case of photo-ionization of a hydrogen-like system consisting of one electron in the field of charge Ze of an ion, the total bound–free absorption cross section σ_v for a photon of frequency v is

$$\sigma_v \sim \frac{Z^4}{v^3 n^5}\ \mathrm{cm}^2, \tag{1.130}$$

where n is the principal quantum number of the initial state. To compute the total opacity, the number density of atoms in the n-th excited state, N_n, has to be considered. The result is

$$\kappa_{\mathrm{bf}}^{v} \sim \sum \frac{N_n \sigma_v}{\varrho}\ \mathrm{cm}^2\, \mathrm{g}^{-1}. \tag{1.131}$$

From this, the Rosseland mean opacity due to bound–free transitions only can be derived. An usual approximation is

$$\kappa_{\mathrm{bf}} = 4.32 \times 10^{25}\, Z\, (1 + X_{\mathrm{H}})\, \varrho\ T^{-7/2}\, \mathrm{cm}^2\, \mathrm{g}^{-1}, \tag{1.132}$$

where now Z is the mass fraction of elements heavier than helium. Note that this opacity is of the form of Kramers opacity.

Line absorption resulting from photon-induced transitions between bound levels in atoms or ions, the so-called bound–bound transitions, importantly contributes to the total opacity at temperatures below $\sim 10^6$ K. The bound–bound cross section is given by

$$\sigma_v^{\mathrm{bb}} = \frac{\pi^2 e^2}{m_{\mathrm{e}} c} f_{ij} \phi_v, \tag{1.133}$$

where f_{ij} is the oscillator strength of the transition from state i to j. This coefficient represents how strongly the line absorbs. Finally, ϕ_v is the line profile function. Because of the large number of transitions (typically a few million lines) that must be taken into account,

bound–bound transitions represent a major complication in opacity calculations. Thermal and pressure broadening effects are important and the total absorption coefficient critically depends on temperature.

Negative hydrogen ions, H^-, provide another source of opacity. The hydrogen atom can harbor a second electron in a bound state with a binding energy of only 0.7544 eV. This energy being so small means that the H^- ion will be easily ionized if temperatures exceed a few thousand degrees. In fact, all photons with wavelengths $\lambda < 1.65\,\mu$m have enough energy to ionize the H^- ion back to a neutral hydrogen atom plus a free electron. Additionally, it is clear that the total opacity must be proportional to the electron density. However, it also has to be taken into account that the electrons needed to form H^- come from ionized metals. According to these considerations it turns out that in hot stars the H^- ion is so rapidly ionized that this source of opacity is not relevant. On the contrary, in cool stars there are too few free electrons (since no ionized metals are present) to form H^- ions, so the contribution to the opacity is negligible as well, whereas for solar-like stars the H^- ion is the dominant source of continuum opacity at optical wavelengths. In particular, the opacity due to the negative hydrogen ion is the most important source of opacity in the solar atmosphere.

For temperatures lower than $\approx$5,000 K, the contribution from molecules becomes a relevant opacity source. The contributions to molecular opacity arise from transitions between rotational and vibrational molecular states, which are very frequent at these very low temperatures, typical, for instance, of late-type main sequence stars and cool red giants. Also the formation of small dust grains at even lower temperatures ($\approx$1,700 K) has to be considered in the opacities needed to compute reliable atmosphere models of cool stars.

As stems from the preceding paragraphs, which is the dominant source of opacity depends very much on the thermodynamical state of stellar matter. In general, at low temperatures, bound–bound and bound–free processes totally dominate the opacity. At larger temperatures, when ionization is almost complete, free–free transitions take over and become the most important source of opacity. These processes become less relevant at even larger temperatures, where scattering by free electrons is the major source of opacity. Needless to say, all opacity processes contribute simultaneously to the total opacity, and to compute the resulting value of the radiative opacity, κ_{rad}, the sum of the contributions of the monochromatic opacities resulting from all the processes described so far has to be done. After doing that, the integral in (❯ 1.24) must be computed. It is important to realize at this point of our discussion that the sum of the Rosseland mean opacities of each opacity component is not equal to the Rosseland mean of the sum. Hence, the Rosseland mean of a given process lacks meaning, except in the particular case in which the corresponding process dominates by far the rest of the contributions to the opacity. For typical stellar compositions, the largest values of the radiative opacity occur for temperatures between $\sim 10^4$ and 10^5 K, corresponding to the temperatures appropriate to ionize hydrogen and helium, the principal constituents of stellar matter.

Several groups have computed detailed frequency-averaged opacities. Among them the most reliable and frequently used opacities are those of the OPAL (Rogers and Iglesias 1992) and of the OP (Seaton et al. 1994) projects. Both projects have presented their calculations in the form of extensive tabulations for different chemical compositions for a wide range of temperatures and densities. At very low temperatures the most up-to-date and comprehensive set of opacity data has been assembled by Ferguson et al. (2005). Their opacities cover temperatures between 30,000 and 500 K, and, in addition to the usual continuous absorbers, include atomic and molecular line absorption, and grain absorption and scattering (by silicates, iron, carbon, and SiC). More recently, Lederer and Aringer (2009) have presented calculations of Rosseland

opacities for low temperatures that consider the effects of varied abundances of carbon and nitrogen for different metallicities.

6.3.2 Conduction

At the high densities found in the core of evolved stars, the main mechanism of energy transfer is not radiation but conduction by degenerate electrons. For the conditions found in the deep cores of these stars, the mean-free path of electrons is usually very large. This is so because after an interaction in which an electron is involved its energy is in most cases below the Fermi level. Consequently, since below the Fermi energy all the levels are occupied, the electron has to travel long distances to release the excess energy absorbed in the interaction. Of course, this only occurs when $k_B T \ll \varepsilon_F$, that is, in conditions of strong degeneracy. Hence, electrons can transport energy very efficiently and the related opacity is small ($\kappa \sim 1/\ell$). It can be shown that, for strong degeneracy, an approximate expression for the conductive opacity is

$$\kappa_{cd} \sim 5 \times 10^{-3} \frac{\sum Z_j^2 X_j \theta_j / A_j}{(1 + X_H)^2} \frac{T_7^2}{(\varrho/10^5)^2} \ cm^2 g^{-1}, \tag{1.134}$$

where $\theta_j \sim 0.85/Z_j^{1/3}$, T_7 is the temperature in units of 10^7 K, and X_j the abundance by mass of element j. Note that the larger the density, the smaller the conductive opacity. The reason for this is that, as already explained, for strong degeneracy it becomes very difficult for an electron to scatter, with the consequent result that the mean-free path becomes very long. For helium composition and $T \sim 10^7$ K and $\varrho \sim 10^5$ g cm^{-3}, the conductive opacity is two orders of magnitude smaller than the electron scattering opacity (κ_{es}). Accordingly, the total opacity given by (❷ 1.31) is very small, of the order of $10^{-2}\kappa_{es}$. Finally, it is rather evident from the previous discussion that at low densities, electrons transport little energy compared to photons.

More elaborated prescriptions than that given by (❷ 1.134) are available in the referenced literature. In particular, detailed calculations of conductive opacities for a wide range of stellar conditions have been given by Itoh et al. (1983). This set of conductive opacities is the most commonly adopted in nearly all the state-of-the-art stellar evolutionary codes. However, there are other prescriptions, the most recent one being that of Cassisi et al. (2007). These authors provide determinations of the conductive opacity covering the entire parameter space relevant to stellar evolution models (i.e., both the regime of partial and high electron degeneracy).

6.4 Neutrino Losses

Photons are not the only way in which energy is lost from stars. Neutrinos also play an important role, especially during the last stages of stellar evolution. These weakly interacting particles escape freely from the dense cores of evolved stars – except in the case of core-collapse supernovae, where the densities are extremely high – carrying out copious amounts of energy. This is because under most circumstances (but in those found in the central very dense regions of these supernovae) their interaction cross section with matter is extremely small ($\sim 10^{-44}x^2$ cm^2, x being the neutrino momentum in units of MeV/c). Thus, their mean-free paths are very large and, hence, they can be considered as an instantaneous sink of energy for most stellar evolutionary stages. According to this discussion, (❷ 1.18) must be correspondingly modified to include an additional term $-\epsilon_\nu$, which acts as an instantaneous sink of energy.

Besides the nuclear processes in which neutrinos are produced as a regular product of the reaction – like electron captures or the several reactions described in ❯ Sect. 6.2, where the neutrino energy loss is already included in the nuclear energy released – there are four typical processes in which neutrinos are produced as a result of purely leptonic processes: the photoneutrino, plasmaneutrino, pair annihilation, and bremsstrahlung processes, respectively. In the photoneutrino process the outgoing photon in a regular Compton scattering is substituted by the emission of a neutrino–antineutrino pair. In the plasmaneutrino process a photon moving in the electron gas – the so-called plasmon – is transformed in a neutrino–antineutrino pair. Pair annihilation neutrinos are produced at very high temperatures ($T > 10^9$ K) in the reaction $e^- + e^+ \rightleftharpoons \nu_e + \bar{\nu}_e$, instead of a normal photon. Finally, the emission of a neutrino–antineutrino pair due to the interaction of a high-energy electron with a heavy nucleus is known as the neutrino bremsstrahlung process, where again the photon is replaced by the neutrino pair. Additionally, there is a less common neutrino process, which only occurs for nuclei with relatively large values of Z and at low densities and temperatures – a situation not commonly found in stellar interiors – which is the recombination neutrino process. In this process an electron in the continuum makes a transition to a bound state and a neutrino pair is emitted.

Analytic expressions for all these processes as a function of the density, the temperature, and the chemical composition have been compiled by Itoh et al. (1996). For the sake of conciseness and given that these analytical expressions incorporate coefficients that depend on the detailed chemical composition – which are listed in lengthy tables – their results will not be reproduced here. Instead, the interested reader is referred to their paper. These neutrino emission rates are the most commonly used in stellar evolutionary calculations. However, other expressions can be found in the specialized literature – see, for instance, Haft et al. (1994).

7 Other Physical Processes

During some evolutionary phases there are other physical processes which become of the maximum importance. This is especially true for compact stars, and specifically for white dwarfs, for which element diffusion and radiative levitation are crucial. Element diffusion is of the maximum importance to understand the observed purity of white dwarf atmospheres. The very large surface gravities of these stars makes elements heavier than hydrogen to settle down over timescales shorter than the evolutionary ones, leaving behind pure hydrogen or helium atmospheres. In these stars, the interfaces between the hydrogen (if present) and helium layers, and between the helium buffer and the core are the product of element diffusion. The study of element diffusion processes in white dwarfs dates back to the early studies of Schatzman (1958). Since then, numerous studies have been devoted to this subject, and have convincingly demonstrated that gravitationally induced diffusion is an extremely efficient process in the envelopes of white dwarfs.

Under the influence of gravity, partial pressure, thermal gradients, and induced electric fields, the diffusion velocities in a multicomponent plasma satisfy a set of $N - 1$ independent linear diffusion equations (Burgers 1969):

$$\frac{dp_i}{dr} - \frac{\varrho_i}{\varrho}\frac{dp}{dr} - n_i Z_i e E = \sum_{j \neq i}^{N} K_{ij}\left(w_j - w_i\right) + \sum_{j \neq i}^{N} K_{ij} z_{ij} \frac{m_j r_i - m_i r_j}{m_i + m_j}, \tag{1.135}$$

coupled with the equation of heat diffusion:

$$
\begin{aligned}
\frac{5}{2} n_i k_{\mathrm{B}} \nabla T = {}&- \frac{5}{2} \sum_{j \neq i}^{N} K_{ij} z_{ij} \frac{m_j}{m_i + m_j} \left(w_j - w_i \right) - \frac{2}{5} K_{ii} z_{ii}'' r_i \\
&- \sum_{j \neq i}^{N} \frac{K_{ij}}{\left(m_i + m_j \right)^2} \left(3 m_i^2 + m_j^2 z_{ij}' + 0.8 m_i m_j z_{ij}'' \right) r_i \\
&+ \sum_{j \neq i}^{N} \frac{K_{ij} m_i m_j}{\left(m_i + m_j \right)^2} \left(3 + z_{ij}' - 0.8 z_{ij}'' \right) r_j.
\end{aligned}
\tag{1.136}
$$

In these equations p_i, ϱ_i, n_i, Z_i, and m_i denote, respectively, the partial pressure, mass density, number density, and charge and mass of chemical species i, N is the number of ionic species plus the electron, and the rest of the symbols have their usual meaning. The unknown variables are the diffusion velocities with respect to the center of mass, w_i, and the residual heat flows r_i. In addition, the electrical field E has to be determined. The resistance coefficients K_{ij}, z_{ij}, z_{ij}', and z_{ij}'' must also be provided (Paquette et al. 1986a, b) to solve these equations. In total there are $2N - 1$ equations and $2N + 1$ unknowns. The equations for no net mass flow and no electrical current provide two additional conditions that must be fulfilled:

$$
\sum_i A_i n_i w_i = 0
\tag{1.137}
$$

$$
\sum_i Z_i n_i w_i = 0.
\tag{1.138}
$$

❯ Equation 1.135 can be manipulated to obtain:

$$
\frac{1}{m_i} \left[\sum_{j \neq i}^{N} K_{ij} \left(w_- w_j \right) + \sum_{j \neq i}^{N} K_{ij} z_{ij} \frac{m_i r_j - m_j r_i}{m_i + m_j} \right] - Z_i e E = \alpha_i - k_{\mathrm{B}} T \frac{d \ln n_i}{dr},
\tag{1.139}
$$

where

$$
\alpha_i = -A_i m_{\mathrm{H}} g - k_{\mathrm{B}} T \frac{d \ln T}{dr},
\tag{1.140}
$$

g being the gravitational acceleration. The unknowns w_i, r_i, and E can be written in terms of the gradient of ion densities (similarly for r_i and E):

$$
w_i = w_i^{\mathrm{gt}} - \sum_j \sigma_{ij} \frac{d \ln n_j}{dr},
\tag{1.141}
$$

where w_i^{gt} stands for the velocity component resulting from gravitational settling and thermal diffusion, and the summation is done *for the ions only*. This equation, together with (❯ 1.136– 1.138) can be solved using matrix inversion to find w_{ij}^{gt} and σ_{ij}, which finally are employed to follow the evolution of the ionic species:

$$
\frac{\partial n_i}{\partial t} = -\frac{1}{r^2} \frac{\partial}{\partial r} \left[r^2 \left(w_{ij}^{\mathrm{gt}} n_i - \sum_j \frac{n_i}{n_j} \sigma_{ij} \frac{\partial n_j}{\partial r} \right) \right].
\tag{1.142}
$$

In the otherwise pure atmospheres of white dwarf stars there are occasional appearances of other elements. Consequently, a competing mechanism to gravitational diffusion must be at work. One of these is radiative levitation, especially for hot white dwarfs – those with effective temperatures larger than ~20,000 K. The physical principle operating here is that ions with large

charges have larger cross sections and, thus, absorb more photons. This is done usually through bound–bound interactions, the net effect being that these ions acquire momentum from the radiation field, thus leading to differential accelerations that make them appear on the surface of the star. In virtually all recent calculations it is assumed that a given levitating element is trace. That is, it is assumed that its abundance has no relevant influence on the structure of the star. Additionally, it is assumed that the approximation of equilibrium abundances holds, and thus that the radiative acceleration can be equated to the local effective gravity at each mass shell of the envelope. To solve for the abundances the total radiative acceleration for element i through bound–bound absorption,

$$g_i^{\mathrm{rad}} = \frac{4\pi}{c} \frac{1}{X_i} \sum_j \sum_{k>j} \int_0^\infty \kappa_i^{jk}(\nu) H_\nu d\nu \qquad (1.143)$$

must be computed. In this expression X_i is the mass fraction of the corresponding element, κ_i^{jk} is the monochromatic opacity due to the bound–bound absorption from state j to level k, and H_ν is the monochromatic Eddington flux. In local thermodynamic equilibrium,

$$\kappa_i^{jk}(\nu) = \frac{N_i^j}{\varrho} \frac{\pi e^2}{m_e c} f_i^{jk} \phi_i^{jk}(\nu) \left(1 - e^{-h\nu/k_B T}\right), \qquad (1.144)$$

where N_i^j is the number density of ions of type i in excitation state j, f_i^{jk} is the oscillator strength of the bound–bound transition from j to k, and ϕ_i^{jk} is the normalized line profile of such transition. This acceleration must be equated for each ion to the local gravity at each mass shell. Clearly, computing radiative accelerations requires improved oscillator strengths and reliable atomic data. Modern calculations (Chayer et al. 1995) rely on the data bank TOPBASE (Cunto and Mendoza 1992), associated with the Opacity Project (Seaton et al. 1994).

There are other physical processes that affect stellar evolution like mass loss, rotation, and magnetic fields. Mass loss is relevant in giant and luminous stars and it is important to explain some observations. On the other hand, stars are observed to rotate. Rotation affects star evolution particularly via the associated meridional circulation and other processes that lead to chemical mixing – see Maeder (2009). Additional physical processes associated with changes in the chemical abundance distribution may affect the evolution of evolved star. This is the case of old and cool white dwarf stars, where the gravitational energy released during carbon-oxygen phase separation upon crystallization constitutes an additional source of energy that markedly impacts the cooling times of these stars (Isern et al. 2000).

8 Boundary Conditions and Stellar Atmospheres

As it will be shown below, to integrate the equations of stellar structure, boundary conditions are needed at both the stellar center and the surface. At the stellar center, that is, at $m = 0$, both the radius and the luminosity vanish. This leads to singularities. It is not difficult to show that near the center a first-order Taylor expansion of the equations of stellar structure previously derived in ❯ Sects. 2–4 yields

$$r = \left(\frac{3}{4\pi\varrho_c}\right)^{1/3} m_c^{1/3} \qquad (1.145)$$

$$P = P_c - \frac{3G}{8\pi}\left(\frac{4\pi\varrho_c}{3}\right)^{4/3} m_c^{2/3} \tag{1.146}$$

$$l = \left(\varepsilon_{\text{nuc}} - \varepsilon_\nu + \varepsilon_g\right)_c m_c \tag{1.147}$$

$$T^4 = T_c^4 - \frac{1}{2ac}\left(\frac{3}{4\pi}\right)^{2/3} \kappa_c \left(\varepsilon_{\text{nuc}} - \varepsilon_\nu + \varepsilon_g\right)_c \varrho_c^{4/3} m_c^{2/3} \quad \text{(radiative)} \tag{1.148}$$

$$\ln T = \ln T_c - \left(\frac{\pi}{6}\right)^{1/3} G \frac{\nabla_{\text{ad},c}\, \varrho_c^{4/3}}{P_c} m_c^{2/3} \quad \text{(convective)}, \tag{1.149}$$

where the suffix "c" means the central values of the physical variables and m_c is the mass of the central sphere.

The treatment of the surface conditions is more difficult, partly because it involves the difficult issue of how energy is transported in the very outer layers of the star. At the surface, $m = M$ and $l = L$, where L is the surface luminosity that has to be determined. Deriving the boundary conditions at the surface requires the computation of model atmospheres. Usually, the Eddington gray approximation for radiative transfer in the case of plane-parallel geometry is used:

$$\frac{dP}{d\tau} = \frac{g}{\kappa_{\text{rad}}} \tag{1.150}$$

$$T^4 = \frac{3}{4}\, T_{\text{eff}}^4\left(\tau + \frac{2}{3}\right) \tag{1.151}$$

where g is the surface gravity and τ is the optical depth, defined by $d\tau = \kappa_{\text{rad}}\, \varrho\, dr$. The first of these equations corresponds to the equation of hydrostatic equilibrium. Integration of these two equations from starting values ($P \approx 0$, $T \approx 0$ at $\tau = 0$) down to $\tau = 2/3$ yields P_s. The layer at $\tau = 2/3$ defines the location of the photosphere from which most of the radiation is emitted into the space. There the temperature is $T = T_{\text{eff}}$, where T_{eff} is the effective temperature of the star, which is defined by the relation $L_s = 4\pi R^2 \sigma\, T_{\text{eff}}^4$, $\sigma = ac/4$ being the Stefan–Boltzmann constant. Note that T_{eff} corresponds to the temperature of a blackbody that has the same energy flux of the real star. From here, a two-parameter set of boundary conditions between T_{eff}, P_s, L_s, and R can be cast. For instance, assuming arbitrary values of R and L_s all the other values at the surface can be obtained. In fact, from the values of R and L_s, the value of T_{eff} is determined. Also, the value of g is obtained as well, since the total stellar mass is given. This information together with the chemical composition of the atmosphere (which is assumed to be the same as the composition of the outer layers, and thus known) allows to integrate the model atmosphere and to find P_s.

Finally, it is worth mentioning that during certain stages of evolution, a better treatment for the outer layers than that given by the Eddington approximation is needed. This is the case for instance in giant stars, where the effects of sphericity are usually considered. In cool and dense atmospheres, like those of white dwarfs, the results from full non-gray model atmospheres that take into account convection has to be considered. This is necessary for a proper determination of the envelope structure as well as the cooling time of such stars.

9 Numerical Techniques: Modern Implementations

The basic equations that govern the structure and evolution of a spherically symmetric star in hydrostatic equilibrium have been derived in ❯ Sects. 2–4. In terms of the Lagrangian variable, m, they can be written as

$$\frac{\partial r}{\partial m} = \frac{1}{4\pi r^2 \varrho} \tag{1.152}$$

$$\frac{\partial P}{\partial m} = -\frac{Gm}{4\pi r^4} \tag{1.153}$$

$$\frac{\partial l}{\partial m} = \varepsilon_{\text{nuc}} - \varepsilon_\nu - C_P \frac{\partial T}{\partial t} + \frac{\delta}{\varrho} \frac{\partial P}{\partial t} \tag{1.154}$$

$$\frac{\partial T}{\partial m} = -\frac{GmT}{4\pi r^4 P} \nabla. \tag{1.155}$$

To this set of equations, the equation for the variation of chemical composition with time has to be added. This, for radiative regions, must be done using the set of equations presented previously in ❯ Sect. 6.2.4 – see (❯ 1.120) – whereas if chemical changes are due to different mixing processes, a diffusion-like set of equations must be used:

$$\left(\frac{\partial Y_i}{\partial t}\right) = \left(\frac{\partial Y_i}{\partial t}\right)_{\text{nuc}} + \frac{\partial}{\partial m}\left[(4\pi r^2 \varrho)^2 D \frac{\partial Y_i}{\partial m}\right], \tag{1.156}$$

where the first term represents the chemical changes due to nuclear reactions and the second one provides the changes of the chemical abundances resulting from mixing processes, which are characterized by a diffusion coefficient D. In general, the equations for the abundance changes are decoupled from the set of equations providing the thermal and mechanical changes, namely, (❯ 1.152– 1.155). This is a valid assumption only in the case in which the nuclear timescale is much larger than the other relevant timescales of the star. This allows to treat the problem by solving first (❯ 1.152– 1.155) at a given time t_0 and for a given chemical composition. Then the change in chemical composition during the time step Δt – that is, the chemical composition at time $t_0 + \Delta t$ – is obtained using the physical variables determined at t_0. Afterward the new chemical compositions are used recursively to find the new physical variables at $t_0 + \Delta t$, and so on. However, in some advanced stages of evolution, where the changes of chemical compositions occur in timescales comparable to that of the physical variables, decoupling the equations for the chemical changes from the other four equations is not a realistic assumption. The term ε_ν in (❯ 1.154) represents the energy losses by neutrino in erg g^{-1} s^{-1}, as discussed in ❯ Sect. 6.4. As mentioned, for most stellar conditions, neutrinos do not interact with matter, thus they only act as an energy sink of energy at the location where they are produced. In (❯ 1.155), $\nabla = \nabla_{\text{rad}}$ – as given by (❯ 1.33) – if the energy transport is done by radiation (and conduction). In the case where energy transport is due to convection, $\nabla = \nabla_{\text{conv}}$, where ∇_{conv} is specified by the adopted treatment of convection. In addition, the functions that describe the properties of stellar matter – ϱ, δ, α, C_P, ∇_{ad}, ε_{nuc}, ε_ν, κ_{tot}, and ∇_{conv} – that depend on P, T, and chemical composition, must be specified.

❯ Equations 1.152– 1.155 constitute a set of nonlinear, partial differential equations that have to be integrated numerically. The independent variables are the mass coordinate m, which runs from zero to the value of the total mass M – the index r is dropped in the notation – and t.

To solve these equations, the total mass M of the star and proper initial values, usually only the chemical composition at the initial instant t_0, together with appropriate boundary conditions at $m = 0$ and $m = M$ must be specified. These boundary conditions have been discussed previously, in ❯ Sect. 8. The solution for r, P, l, T, and chemical composition at a given time in the whole mass interval is named a *stellar model*.

A standard technique for solving the equations of stellar structure and evolution is based on an iterative implicit technique, the so-called the Henyey method or relaxation method, in which the differential equations are replaced by a set of difference equations in a discrete number of mass shells (or grid). Here, an initial or approximate solution is gradually improved by applying successive simultaneous corrections to all variables at all points on the grid. The corrections to the physical variables are applied until they become insignificant and the initial model "relaxes" to the correct one. To implement the technique, the star is divided into N concentric mass shells (very few stellar evolutionary codes use the radius as independent variable), each of them labeled with the lagrangian coordinate m_j, where $m_1 = 0$ and $m_N = M$. In addition, the time derivatives appearing in (❯ 1.154) are usually replaced at any point j of the grid by

$$\left(\frac{dP}{dt}\right)_{j+1/2} = \frac{P_{j+1/2} - P^*_{j+1/2}}{\Delta t} \tag{1.157}$$

$$\left(\frac{dT}{dt}\right)_{j+1/2} = \frac{T_{j+1/2} - T^*_{j+1/2}}{\Delta t}, \tag{1.158}$$

where P^* and T^*, evaluated at the middle of the mass interval, denote the values of P and T at the earlier time $t_o - \Delta t$, and are, thus, known quantities. With these considerations, (❯ 1.152–1.155) are converted to a set of ordinary differential equations, which can be replaced by the corresponding difference equations. For instance, the equation of hydrostatic equilibrium is replaced by the following difference equation:

$$\frac{P_{j+1} - P_j}{m_{j+1} - m_j} = -\frac{G}{4\pi} \frac{m_{j+1/2}}{r^4_{j+1/2}}, \tag{1.159}$$

where $r_{j+1/2} = (r_{j+1} + r_j)/2$ and $m_{j+1/2} = (m_{j+1} + m_j)/2$. For each mass shell j, the resulting four difference equations ($i = 1, 4$) can be written in the form

$$G^i_j \equiv \frac{y^i_{j+1} - y^i_j}{m_{j+1} - m_j} - f_i\left(y^1_{j+1/2}, \ldots, y^4_{j+1/2}\right) = 0, \tag{1.160}$$

where $y^1 = r$, $y^2 = P$, $y^3 = l$, and $y^4 = T$. The index j runs from 2 to $N - 1$. At the center ($j = 1$), singularities occur. There, the radius and luminosity vanish, that is, $r = 0$ and $l = 0$. As already shown – see ❯ Sect. 8 – the boundary conditions at the center ($j = 1$) can be obtained by performing a Taylor expansion of (❯ 1.152) and (❯ 1.153) – see (❯ 1.145– 1.149) – and it can be easily shown that they adopt the form

$$C^i\left(y^1_2, y^2_2, y^3_2, y^4_2, y^2_1, y^4_1\right) = 0, \tag{1.161}$$

with $i = 1, 4$. As for the boundary conditions at the surface ($j = N$) – see ❯ Sect. 8 – the following equations can be established:

$$S^1 \equiv y^2_N - h_s\left(y^1_N, y^3_N\right) = 0 \tag{1.162}$$

$$S^2 \equiv y_N^4 \; - \; q_s(y_N^1, y_N^3) = 0. \tag{1.163}$$

Usually, a linear approximation is considered for the functions h_s and q_s. Thus, only three integrations of the model atmosphere – (❷ 1.150) and (❷ 1.151) – are needed to find all the coefficients that define h_s and q_s.

Note that the total number of unknowns is $4N - 2$ and the total number of equations is also $4N - 2$. Consider now a given time t and assume that $(y_j^i)_1$ with $i = 1, \ldots, 4$ and $j = 1, \ldots, N$ is a first approximation to the solution of the set of equations, which as a first guess may be taken as the solution at the previous time $t - \Delta t$. Since the values of $(y_j^i)_1$ are only an approximation to the solution to the set of equations and not the real one, it is clear that $G_j^i(1) \neq 0$, $C^i(1) \neq 0$, and $S^{1,2}(1) \neq 0$. Here, the label "1" refers to the initial guess. Let now δy_j^i be the corrections to all variables at all mass points. A second approximation can be then obtained:

$$(y_j^i)_2 = (y_j^i)_1 \; + \; \delta y_j^i, \tag{1.164}$$

so that now $G_j^i(2) = 0$, $C^i(2) = 0$, and $S^{1,2}(2) = 0$. If the corrections are small, a first-order Taylor expansion yields:

$$G_j^i(1) + \sum_{m=1}^{4} \frac{\partial G_j^i}{\partial y_j^m} \, \delta y_j^m + \sum_{m=1}^{4} \frac{\partial G_j^i}{\partial y_{j+1}^m} \, \delta y_{j+1}^m = 0 \qquad i = 1, \ldots, 4 \quad j = 2, \ldots, N - 1, \tag{1.165}$$

and similarly for (❷ 1.161), (❷ 1.162), and (❷ 1.163). The derivatives of G_j^i are evaluated using the first approximation as arguments. From here, the corrections δy_j^i can be found after inverting a band-type matrix (Henyey matrix) which has nonvanishing elements only in blocks near the diagonal (Henyey et al. 1959, 1964; Larson and Demarque 1964; Nobili and Turolla 1988). Indeed, note that difference equations depend only on variables at adjacent points. This fact enormously simplifies the inversion technique to find the corrections δy_j^i. After consecutive iterations, the approximate solution can be improved until the absolute value of all corrections drops below a given limit or difference equations are satisfied to the desired accuracy. To compute an evolutionary sequence, after convergence of the model at time t, a new time step is determined, the chemical composition for the new time is assessed from the stellar model converged at t, which is also used as an initial solution for the new time. The Henyey technique is a relaxation technique, and has proved to be extremely efficient and stable. It should be stressed, however, that the equations of stellar structure and evolution are strongly nonlinear, so it is expected that, since the corrections are obtained from linearized equations, the solution requires several iterations in some cases, particularly if the initial approximation is not a good representation of the solution or if the time step is not small enough. Nevertheless, in most cases, only few iterations are needed to find the solution.

10 State-of-the-Art Modeling

Building a state-of-the-art stellar evolutionary code requires large efforts. As has been made clear in ❷ Sect. 6, detailed physical inputs are required to produce reasonable models. Not only that, it has also been shown in ❷ Sect. 9 that the system of differential equations that governs the structure and evolution of stars must be solved using specific techniques. This, as mentioned earlier, is a tough task as it involves the solution of a boundary problem.

There are several existing evolutionary codes which incorporate reliable solvers of the equations of stellar structure and up-to-date physical inputs. Among these it is worth mentioning, in alphabetical order, the following ones, but the reader should keep in mind that this list is not intended to be exhaustive whatsoever:

- ASTEC – Aarhus STellar Evolution Code (Christensen-Dalsgaard 1982)
- CESAM – Code d'Evolution Stellaire Adaptatif et Modulaire (Morel and Lebreton 2008)
- DSEP – Darmouth Stellar Evolution Program (Chaboyer et al. 2001)
- EVOL (Blöcker 1995; Herwig 2000)
- EVOLVE (Iben 1965), which was subsequently modified to follow carbon burning (García-Berro and Iben 1994)
- GARSTEC – Garching STellar Evolution Code (Weiss and Schlattl 2008)
- FRANEC – Frascati Raphson Newton Evolutionary Code, of which there are several versions, see for instance Pietrinferni et al. (2004)
- GENEC – Geneva Evolution Code (Meynet and Maeder 2000)
- KEPLER (Heger et al. 2000; Weaver et al. 1978)
- LPCODE – La Plata Stellar Evolutionary Code (Althaus et al. 2005)
- MESA – Modules for Experiments in Stellar Astrophysics (Paxton et al. 2011)
- STARS (Pols et al. 1995)
- STERN (Heger et al. 2000; Langer 1998)
- TGEC – Toulouse-Geneva Evolution Code (Richard et al. 1996)
- TYCHO (Young and Arnett 2005)
- YREC – Yale Rotating Stellar Evolution Code (Demarque et al. 2008).

Fortunately, some of these codes are freely available on the Internet – although, of course, some work must be done to adapt them to the specific problem under study – whereas others can be used with permission of the original authors. Finally, others are proprietary codes and permission to use them is not granted.

Describing in detail the variety of physical inputs adopted in each one of these stellar evolutionary codes is beyond the scope of this chapter, so the interested reader is referred to the cited literature. However, a few words regarding the general features of these codes are in order. There are some codes that are specialized at following the initial stages of stellar evolution, for instance ASTEC. Many others are able to follow only the hydrogen and helium burning phases and the thermal pulses on the Asymptotic Giant Branch, but are not able to follow in a detailed and realistic way the carbon burning phase – FRANEC and GARSTEC are good examples, but not the only ones – however they perform extremely well at producing realistic sets of isochrones, while others are specialized in following specific evolutionary stages, for instance the white dwarf evolutionary phase – the leading example is LPCODE – and they produce very accurate cooling tracks. Other codes (GNEC and YREC) incorporate the effects of slow rotation. Finally, other codes are more suitable to follow the evolution of massive stars all the way to the supernova stage – KEPLER being an example of these type of codes. Also, most of the freely available stellar evolutionary codes, but a few ones, rely on gray atmospheres and some adaptations must be made to incorporate non-gray detailed atmospheres.

It is also important to mention that although all these codes are specifically adapted to the research needs and interests of the authors and, consequently, the physical inputs are, as previously said, extremely diverse, there are as well a set of basic ingredients which are common to all of them. One of these is the usage of the OPAL opacities previously discussed in ❯ Sect. 6.3. The most up-to-date stellar codes use this set of opacities, which are a reference in the field.

However, prescriptions for the convective instability are very different from one another, as also are other physically interesting inputs. Specifically, most stellar evolutionary codes use the classical mixing length treatment of Böhm-Vitense (1958) and the onset of convection is determined according to the Schwarzschild criterion ($\nabla_{ad} - \nabla_{rad} < 0$), see ❯ Sect. 4.3, although some (variable) amount of convective overshooting is allowed to occur, and only very few stellar evolutionary codes incorporate more sophisticated theories of convection. Finally, it is also important to realize that most of these state-of-the-art codes adopt the nuclear reaction rates of the NACRE compilation (Angulo et al. 1999), see ❯ Sect. 6.2, although depending on the size of the nuclear network employed to follow the abundances other sources for the relevant cross sections are implemented. Thus, the results obtained using these stellar evolutionary codes differ sizably from one another, although the general characteristics of the different stellar evolutionary phases agree qualitatively. Anyone trying to pursue the hard task of building a stellar evolutionary code from scratch or to improve a previous version of one of his/her own should be aware that most of the necessary pieces of computer code needed to produce realistic physical inputs can be found on the Web page of the IAU Commission 35.[2] Also, the exact way in which the equations of stellar structure are solved is very different in all the numerical codes. Although all of the previously listed stellar codes share a common feature, namely, that they use Henyey-type techniques, the way in which the equations of stellar structure are discretized varies from one to another code. For instance, most commonly the equations of stellar structure are discretized adopting the interior mass as the independent variable, but some codes adopt the radius as the independent variable. Additionally, the pressure, temperature, luminosity, radius, and interior mass can be all defined at the zone edges, but in some codes the pressure, temperature, and, thus, density are defined midway between l, r, and m. To these differences one must also add the way in which the changes in composition are dealt with, not only in the convective regions, but also in the radiative ones. The most extensively used stellar evolutionary codes employ nuclear networks similar to that introduced in ❯ Sect. 6.2.4, but the variety of implementations is also very large, as it is also the number of isotopes followed during the course of stellar evolution. Finally, the way in which zoning and the choice of adequate time steps is dealt with is also extremely dependent on the particular taste of the programmer. To put just one example of these procedures, most stellar evolutionary codes introduce new mesh points to allow a smooth variation of the relevant physical quantities, say the temperature, density, pressure, luminosity, etc., inside the star. This is done by allowing a maximum fractional change between adjacent mass shells, η, which is typically of the order of a few percent. Most stellar evolutionary codes use this strategy to avoid numerical instabilities, except the STAR evolutionary code, which incorporates additional equations to determine the adequate zoning (Eggleton 1971). The way in which the boundary conditions are introduced also adds differences to the results obtained using each of these evolutionary codes, and the way in which the initial guess for the next time step is computed is very different as well, since in some codes the initial solution is extrapolated (linear, semilogarithmic, etc.) from the previous one, while in some others this initial guess is simply the last computed model (absolutely no extrapolation). Additional fine details include different prescriptions to deal with the boundaries of convective regions, as in some codes the nature of a given mass shell cannot change once it is determined from the initial model (it is always convective or radiative), while in some other codes matter can change from convective to radiative and vice versa in all trials. Finally, it should be mentioned that regions in which an adverse and abrupt temperature gradient forms, implying large

---

[2]http://iau-c35.stsci.edu/Resources/index.html

negative luminosities, are difficult to deal with, and that sometimes it is highly advisable to freeze the mesh during certain periods of time to avoid propagation of numerical errors. The way in which this is done by the different stellar evolutionary codes is highly dependent on the specific way in which the code has been designed and written.

11 Summary

In this chapter, our current understanding of stellar structure has been reviewed. A comprehensive discussion of the equations of hydrostatic equilibrium was given in ❯ Sect. 2, while in ❯ Sects. 3 and ❯ 4 the energy conservation law and the treatment of energy transport – either by radiation, conduction, or convection – were extensively discussed. All these otherwise classical results were treated in detail, and the most commonly used prescriptions were provided. Also, when necessary, the needed references to construct realistic stellar configurations were given as well. With these tools, the virial theorem was introduced in ❯ Sect. 5, which helped to understand the physical behavior of stars.

In the second part of this chapter, the reader was provided with a series of essential physical inputs needed to build a stellar model. This includes, of course, the equation of state, the nuclear reaction rates, the opacities and conductivities, and the neutrino emission rates. This was done in ❯ Sect. 6. Additional physical processes, of special importance for some evolutionary stages, were discussed in ❯ Sect. 7. When possible, the aim was to provide to the interested reader with the most commonly used and/or most reliable or recent physical inputs. As mentioned in ❯ Sect. 1, the intention was to be as complete as possible, without unintentionally missing any key reference.

The subject of stellar atmospheres was superficially treated in ❯ Sect. 8, and, certainly, additional details on this topic are needed, as it was only treated here in connection with the boundary conditions needed to stellar evolution. The reader can find excellent descriptions elsewhere. An approximation to the numerical techniques was given in ❯ Sect. 9, where the most usually adopted technique was described in full detail. To conclude, in ❯ Sect. 10, the most widely used stellar evolutionary codes were critically analyzed.

To conclude we feel necessary to explicitly mention at this point of the discussion that the field of stellar evolution is continuously improving, and most probably several advances during the coming years will be witnessed. More reliable physical inputs will most likely be incorporated to improved versions of the available state-of-the-art stellar evolutionary codes. Better descriptions of convective mixing will become available, an example being the very recent – and impressive – work of Canuto (2011), and companion papers. Certainly, the next decade will see an increase of the predictive power of the theory of stellar structure. Clearly, this will enhance the status of this theory as one of the most important tools for understanding the origin and evolution of our Universe.

Acknowledgments

References

Adelberger, E. G., et al. 2011, Rev Mod Phys, 83, 195

Althaus, L. G., Serenelli, A. M., Panei, J. A., Córsico, A. H., García-Berro, E., & Scóccola, C. G. 2005, A&A, 435, 631

Angulo, C., et al. 1999, Nucl Phys A, 656, 3

Arnett, W. D., & Truran, J. W. 1969, ApJ, 157, 339

Böhm-Vitense, E. 1958, Zeit Astrophysik, 46, 108

Blöcker, T. 1995, A&A, 297, 727

Bravo, E., & García-Senz, D. 1999, MNRAS, 307, 984

Burgers, J. M. 1969, Flow Equations for Composite Gases (New York: Academic)

Canuto, V. M. 2011, A&A, 528, A76

Canuto, V. M., & Mazzitelli, I. 1991, ApJ, 370, 295

Cassisi, S., Potekhin, A. Y., Pietrinferni, A., Catelan, M., & Salaris, M. 2007, ApJ, 661, 1094

Caughlan, G. R., & Fowler, W. A. 1988, Atom & Nucl Data Tables, 40, 283

Chaboyer, B., Fenton, W. H., Nelan, J. E., Patnaude, D. J., & Simon, F. E. 2001, ApJ, 562, 521

Chandrasekhar, S. 1939, An Introduction to the Study of Stellar Structure (Chicago, IL: University of Chicago Press)

Chayer, P., Vennes, S., Pradhan, A. K., Thejll, P., Beauchamp, A., Fontaine, G., & Wesemael, F. 1995, ApJ, 454, 429

Christensen-Dalsgaard, J. 1982, MNRAS, 199, 735

Cox, J. P., & Giuli, R. T. 1968, Principles of Stellar Structure, Vol. I (New York: Gordon and Breach)

Cunto, W., & Mendoza, C. 1992, Revista Mexicana de Astronomisica, 23, 107

Demarque, P., Guenther, D. B., Li, L. H., Mazumdar, A., & Straka, C. W. 2008, Ap&SS, 316, 31

Eddington, A. S. 1916, MNRAS, 77, 16

Eggleton, P. P. 1971, MNRAS, 151, 351

Ferguson, J. W. et al., 2005, ApJ, 623, 585

Freytag, B., Ludwig, H.-G., & Steffen, M. 1996, A&A, 313, 497

García-Berro, E., & Iben, I., Jr. 1994, ApJ, 434, 306

García-Berro, E., Ritossa, C., & Iben, I., Jr. 1997, ApJ, 485, 765

García-Berro, E., Isern, J., & Kubyshin, Y. A. 2007, A&AR, 14, 113

Grossman, S. A., & Taam, R. E. 1996, MNRAS, 283, 1165

Grossman, S. A., Narayan, R., & Arnett, D. 1993, ApJ, 407, 284

Haft, M., Raffelt, G., & Weiss, A. 1994, ApJ, 425, 222

Heger, A., Langer, N., & Woosley, S. E. 2000, ApJ, 528, 368

Henyey, L. G., Wilets, L., Böhm, K. H., Lelevier, R., & Levee, R. D. 1959, ApJ, 129, 628

Henyey, L. G., Forbes, J. E., & Gould, N. L. 1964, ApJ, 139, 306

Herwig, F. 2000, A&A, 360, 952

Iben, I., Jr. 1965, ApJ, 141, 993

Iliadis, C., Longland, R., Champagne, A. E., Coc, A., & Fitzgerald, R. 2010, Nucl Phys A, 841, 31

Isern, J., Mochkovitch, R., García-Berro, E., & Hernanz, M. 1997, ApJ, 485, 308

Isern, J., García-Berro, E., Hernanz, M., & Chabrier, G. 2000, ApJ, 528, 397

Itoh, N., Mitake, S., Iyetomi, H., & Ichimaru, S. 1983, ApJ, 273, 774

Itoh, N., Kuwashima, F., & Munakata, H. 1990, ApJ, 362, 620

Itoh, N., Nishikawa, A., & Kohyama, Y. 1996, ApJ, 470, 1015

Kippenhahn, R., & Weigert, A. 1990, Stellar Structure and Evolution (Heidelberg: Springer)

Kippenhahn, R., Thomas, H. C., & Weigert A. 1965, Z Astrophys, 61, 241

Lane, J. H. 1869, Am J Sci, 50, 57

Langer, N. 1998, A&A, 329, 551

Larson, R. B., & Demarque, P. R. 1964, ApJ, 140, 524

Lederer, M. T., & Aringer, B. 2009, A&A, 494, 403

Longland, R., Iliadis, C., Champagne, A. E., Newton, J. R., Ugalde, C., Coc, A., & Fitzgerald, R. 2010, Nucl Phys A, 841, 1

Maeder, A. 2009, Physics, Formation and Evolution of Rotating Stars (Berlin, Heidelberg: Springer, A&A library)

Meynet, G., & Maeder, A. 2000, A&A, 361, 10

Mihalas, D., & Mihalas, B. W. 1984, Foundations of Radiation Hydrodynamics (New York: Oxford University Press)

Mihalas, D., Hummer, D. G., & Däppen, W. 1988, ApJ, 331, 815

Morel, P., & Lebreton, Y. 2008, Ap&SS, 316, 61

Nobili, L., & Turolla, R. 1988, ApJ, 333, 248

Paquette, C., Pelletier, C., Fontaine, G., & Michaud, G. 1986a, ApJS, 61, 177

Paquette, C., Pelletier, C., Fontaine, G., & Michaud, G. 1986b, ApJS, 61, 197

Paxton, B., Bildsten, L., Dotter, A., Herwig, F., Lesaffre, P., & Timmes, F. 2011, ApJS, 192, 3

Perryman, M. A. C., et al. 2001, A&A, 369, 339

Pietrinferni, A., Cassisi, S., Salaris, M., & Castelli, F. 2004, ApJ, 612, 168

Pols, O., Tout, C. A., Eggleton, P. P., & Han, Z. 1995, MNRAS, 274, 964

Raffelt, G. G. 1999, Annu Rev Nucl Sci, 49, 163

Rauscher, T., & Thielemann, F.-K. 2000, Atom & Nucl Data Tables, 75, 1

Rauscher, T., & Thielemann, F.-K. 2001, Atom & Nucl Data Tables, 79, 47

Richard, O., Vauclair, S., Charbonnel, C., & Dziembowski, W. A. 1996, A&A, 312, 1000

Ritossa, C., García-Berro, E., & Iben, I., Jr. 1996, ApJ, 460, 489

Ritossa, C., García-Berro, E., & Iben, I., Jr. 1999, ApJ, 515, 381

Rogers, F. J., & Iglesias, C. A. 1992, ApJS, 79, 507; ApJ, 456, 902

Rogers, F. J., Swenson, F. J., & Iglesias, C. A. 1996, ApJ, 456, 902

Salpeter, E. E. 1954, Aust J Phys, 7, 373

Schatzman, E. 1958, White Dwarfs (North-Holland: Amsterdam)

Schwarzschild, K. 1906, Göttingen Nachr. 195, 41

Seaton, M. J., Yan, Y., Mihalas, D., & Pradhan, A. K. 1994, MNRAS, 266, 805

Segretain, L., Chabrier, G., Hernanz, M., García-Berro, E., Isern, J., & Mochkovitch, R. 1994, ApJ, 434, 641

Timmes, F. X., & Swesty, F. D. 2000, ApJS, 126, 501

Traxler, A., Garaud, P., & Stellmach, S. 2011, ApJL, 728, L29

Weaver, T. A., Zimmerman, G. B., & Woosley, S. E. 1978, ApJ, 225, 1021

Weiss, A., & Schlattl, H. 2008, Ap&SS, 316, 99

Young, P. A., & Arnett, D. 2005, ApJ, 618, 908

Young, P. A., Knierman, K. A., Rigby, J. R., & Arnett, D. 2003, ApJ, 595, 1114